

Effect of the aniline fragment in Pt(II) and Pt(IV) complexes as anti-proliferative agents. Standard reduction potential as a more reliable parameter for Pt(IV) compounds than peak reduction potential.

*Jorge Leal,<sup>1</sup> Lucia Santos,<sup>2</sup> Diego M. Fernández-Aroca<sup>3</sup>, J. Vicente Cuevas,<sup>4</sup> M. Angeles Martínez,<sup>5</sup> Anna Massaguer,<sup>6</sup> Felix A. Jalón,<sup>1</sup> M. José Ruiz-Hidalgo,<sup>7</sup> Ricardo Sánchez-Prieto,<sup>8</sup> Ana M. Rodríguez,<sup>1</sup> Gregorio Castañeda,<sup>9</sup> Gema Durá,<sup>1</sup> M. Carmen Carrión,<sup>1</sup> Silvia Barrabés,<sup>6</sup> Blanca R. Manzano<sup>1,\*</sup>*

<sup>1</sup> Universidad de Castilla-La Mancha, Departamento de Química Inorgánica, Orgánica y Bioquímica, Facultad de Ciencias y Tecnologías Químicas, IRICA, Avda. C. J. Cela, 10, 13071 Ciudad Real, Spain

<sup>2</sup> Universidad de Castilla-La Mancha, Departamento de Química Física, Facultad de Ciencias y Tecnologías Químicas, Avda. C. J. Cela s/n, 13071 Ciudad Real, Spain.

<sup>3</sup> Universidad de Castilla-La Mancha, Laboratorio de Oncología, Unidad de Medicina Molecular, Centro Regional de Investigaciones Biomédicas. Unidad Asociada de Biomedicina UCLM, Unidad asociada al CSIC, Albacete, Spain.

<sup>4</sup> Universidad de Burgos, Department of Chemistry, Pza. Misael Bañuelos S/N, 09001 Burgos, Spain.

<sup>5</sup> Departament de Química, Universitat de Girona, Maria Aurèlia Capmany 69, 17003 Girona, Spain.

<sup>6</sup> Departamento de Biología, Universitat de Girona, Maria Aurèlia Capmany 40, 17003 Girona, Spain.

<sup>7</sup> Universidad de Castilla-La Mancha, Departamento de Química Inorgánica, Orgánica y Bioquímica, Facultad de Medicina de Albacete. Laboratorio de Oncología, Unidad de Medicina

Molecular, Centro Regional de Investigaciones Biomédicas. Unidad Asociada de Biomedicina UCLM, Unidad asociada al CSIC, Albacete, Spain.

<sup>8</sup> Departamento de Biología del Cáncer, Instituto de Investigaciones Biomédicas De Madrid Alberto Sols (CSIC-UAM). Universidad de Castilla-La Mancha, Departamento de Ciencias Médicas. Facultad de Medicina de Albacete. Unidad Asociada de Biomedicina UCLM, Unidad asociada al CSIC, Albacete, Spain.

<sup>9</sup> Universidad de Castilla-La Mancha, Departamento de Química Analítica y Tecnología de los Alimentos, Facultad de Ciencias y Tecnologías Químicas, Avda. C. J. Cela s/n, 13071 Ciudad Real, Spain

Corresponding author

ORCID number: 0000-0002-4908-4503

Email. [blanca.manzano@uclm.es](mailto:blanca.manzano@uclm.es)

## ABSTRACT

The problems of resistance and side effects associated with cisplatin and other chemotherapeutic drugs has boosted research aimed at finding new compounds with improved properties. The use of platinum(IV) prodrugs is one alternative, although there is some controversy regarding the predictive ability of the peak reduction potentials. In the work described here a series of fourteen chloride Pt(II) and Pt(IV) compounds was synthesised and fully characterised. The compounds contain different bidentate arylazole heterocyclic ligands. Their cytotoxic properties against human lung carcinoma (A549), human breast carcinoma (MCF7) and human colon carcinoma (HCT116 and HT29) cell lines were studied. A clear relationship between the type of ligand and the anti-proliferative properties was found, with the best results obtained for the Pt(II) compound that contains an aniline fragment, (**13**), thus evidencing a positive effect of the NH<sub>2</sub> group. Stability and aquation studies in DMSO, DMF and DMSO/water mixtures were carried out on the active complexes and an in-depth analysis of the two aquation processes, including DFT analysis, of **13** was undertaken. It was verified that DNA was the target and that cell death occurred by apoptosis in the case of **13**. Furthermore, the cytotoxic derivatives did not exhibit haemolytic activity. The reduction of the Pt(IV) compounds whose Pt(II) congeners were active was studied by several techniques. It was concluded that the peak reduction potential was not useful to predict the ability for reduction. However, a correlation between the cytotoxic activity and the standard reduction potential was found.

**Keywords:** Platinum, cancer, heterocyclic ligands, standard reduction potential, aniline, Pt(IV)

### 1. Introduction

Since the discovery of the cytotoxic properties of cisplatin [1], and its approval as an anticancer drug in 1979, numerous Pt compounds have been synthesised as potential drugs with better properties [2–4]. However, 40 years later only two other compounds, carboplatin and

oxaliplatin, have been approved as anticancer drugs worldwide [2]. Nedaplatin, lobaplatin and heptaplatin are being used in Japan, China and South Korea, respectively [5,6]. It is worth noting that all of these compounds contain ammonia or amino groups in the cis position. The effectiveness of the platinum compounds is reflected by the fact that they are used as anticancer agents in 50% of all chemotherapeutic regimens administered in the clinic [7,8]. However, to different degrees these compounds cause several undesirable side effects due to their poor selectivity towards tumoral cells and this fact limits the dose that can be administered to patients [9]. Additionally, intrinsic or acquired drug resistance is also a problem encountered with some of these compounds. It is therefore necessary to design new compounds that may have improved properties when compared to the previously approved anticancer drugs. New types of compounds such as monofunctional platinum drugs [10], trans-configured [11], sterically hindered complexes, complexes with biologically active or targeting ligands, and polynuclear platinum complexes are being explored [12–14].

With the aim of broadening the spectrum of complexes and overcoming the constraining issues of classical platinum complexes, new platinum anticancer derivatives containing different kinds of N-heterocycles have been found to show promising results [15–18]. The replacement in cisplatin of one or both ammonia molecules with other non-leaving N-heterocyclic ligands generally affects the pharmacological behaviour of the drug. The lead compound of the series was picoplatin, in which only one ammonia of cisplatin was replaced with a picoline ligand [19]. Monodentate heterocycles have also been included in trans-dichloro platinum complexes [20,21] or in monofunctional derivatives [22,23], with the phenanthriplatin derivative (*cis*-[Pt-(NH<sub>3</sub>)<sub>2</sub>(phenanthridine)Cl]<sup>+</sup>) as an outstanding example [24]. In the last decade, a great deal of effort has been focused on the substitution of the second ammonia, especially given the remarkable results obtained with the coordination of a bidentate ligand such as DACH (1,2-diaminocyclohexane) as in oxaliplatin. Pyridine-based ligands with other functional groups, e.g., aminophosphonate esters [25], amino-thiazolidinone [26] or benzimidazole [27], amongst others, have been reported and attention has also been drawn to a series of N-heterocyclic ligands with

different levels of hindrance, such as imidazole [28], oxadiazole, oxoisoaporphine or benzothiazole moieties [15].

A promising alternative to reduce the side effects of Pt(II) compounds is the use of Pt(IV) pro-drugs [10,13,29–34]. Pt(IV) complexes have a low-spin  $d^6$  octahedral geometry and are considered to be substitution-inert. As a consequence, reactions with biological nucleophiles are slow and the circulation lifetime in the blood of an administered Pt(IV) prodrug will be higher than that of a Pt(II) complex. This opens the way to oral administration and to the reduction of side effects. Several Pt(IV) compounds have entered clinical trials [29]. The nature and geometry of the equatorial ligands determine the cytotoxicity of platinum(IV) compounds and it is believed that the axial ligands are lost upon reduction, although studies have shown that the resulting Pt(II) species is not always the one expected and it depends on the nature of the reducing agent present [29,35]. Gibson and other authors have reported examples where these axial ligands are bioactive giving rise to multi-action prodrugs [36–39] or targeting entities have been included [29,30]. Sadler and co-workers prepared a series of Pt(IV) complexes with azides to enable their selective activation in tumour tissue by irradiation [40–42].

The redox properties of Pt(IV) complexes have an important influence on their pharmacological profile. Fast reduction could result in high systemic toxicity, whereas very slow reduction could lead to low anticancer activity. Activation by reduction is believed to occur primarily inside the cancer cell by a two-electron reductive elimination reaction with reducing agents such as ascorbic acid or glutathione to give the active Pt(II) compound [29]. A substantial reduction by cellular proteins or NADH has also been reported [43–45]. The nature of the axial ligand affects the reduction potential of the complexes (and also the lipophilicity) and can be tuned to achieve the optimal release of the platinum(II) moiety [31,46]. It has been proposed that the pharmacology of Pt(IV) compounds depends on how readily they are reduced [31]. It has been recently reported that some trans-Platinum(IV) pro-drugs exhibit unusual resistance to reduction by endogenous reductants and blood serum but are rapidly activated inside cells [47]. Different mechanisms of reduction have been proposed [43] but there is some controversy concerning the utility of the reduction potential obtained as the irreversible peak ( $E_p$ ) in the cyclic voltammogram

as a measure of the stability towards biological reducing agents and cytotoxicity. It has been proposed that reduction rates correlate with reduction potentials [31,46] and  $E_p$  could be used to predict in vitro cytotoxicity [48–50], but cases have been reported where the  $E_p$  value is not useful for predicting biological behaviour [30,46,51–54]. Baik and co-workers [55] recently reported that the peak potentials for processes such as the reduction of Pt(IV) compounds, which not only involve electron transfer but also M–L bond cleavage and thus are irreversible, are not appropriate to reflect the reduction thermodynamics of the derivatives and it is more convenient to determine the standard reduction potential ( $E^\ominus$ ) with measurements at different scan rates.

Based on these premises, in the present study we decided to carry out the synthesis, full characterisation and study of the cytotoxicity against several cancer cell lines, as well as other biological properties, of a family of chloride Pt(II) and Pt(IV) complexes containing bidentate chelating N-heterocyclic ligands in order to perform an SAR study. Considering the positive results obtained on using ligands with pyridine or imidazolyl rings, the potential bidentate chelate N<sup>N</sup>' ligands **L1–L7** (Figure 1) were selected. One aim was to analyse the differences in behaviour depending on the presence of an imidazolyl or benzimidazolyl fragment and substituents were also included in the NH group, e.g., methyl or cyanoethyl, to modulate the properties and to determine the benefit of the NH group. In particular, the cyanoethyl fragment (**L3**) has improved the cell permeability of drugs such as various Janus protein tyrosine kinase (JAK) inhibitors [56]. Bearing in mind that the majority of successful drugs contain an amino group and the good activity found in a dichloride platinum complex with a 2(amino-methyl) aniline [57], we also envisaged the inclusion of a ligand with an aniline fragment (**L7**), which led to be the most cytotoxic derivative. The hydrolysis process was studied by DFT analysis for this derivative. The corresponding Pt(IV) compounds were obtained in order to evaluate their cytotoxicity and to ascertain, considering the controversy in the bibliography, whether a correlation could be established in this family between the antiproliferative behaviour and the standard reduction potential.

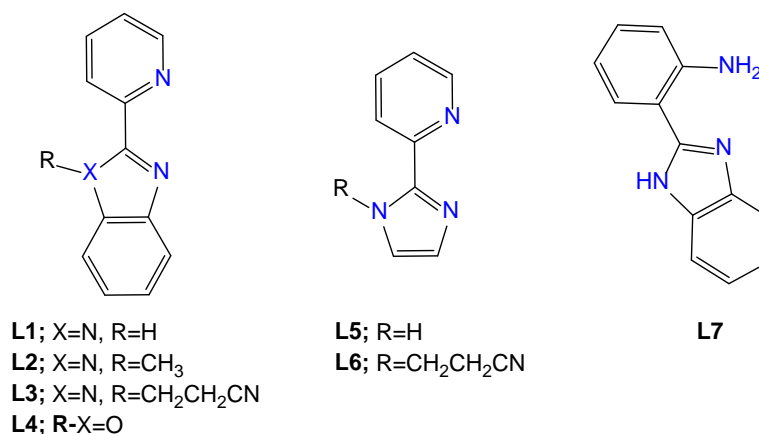


**Figure 1:** Ligands used in this work.

## 2. Experimental Section

### 2.1. Materials and physical methods.

Unless otherwise stated, reagents and solvents used were commercially available and were reagent quality. Solvents and K<sub>2</sub>CO<sub>3</sub> were purchased from Scharlab. Deuterated solvents were purchased from Eurisotop. K<sub>2</sub>[PtCl<sub>4</sub>] was purchased from Johnson Matthey PLC. **L1**, **L4**, **L5** and **L7** were purchased from Sigma-Aldrich. **L2** [58], **L3** [59] and **L6** [59] were prepared according to the literature.

All synthetic manipulations were performed under an inert, oxygen-free, dry nitrogen atmosphere using standard Schlenk techniques. Solvents were distilled from the appropriate drying agents and degassed before use. Elemental analyses were performed on a Thermo Quest FlashEA 1112 microanalyser. The analytical data for the new complexes were obtained from crystalline samples where possible. IR spectra were recorded on a Shimadzu IR Affinity- 1S IR spectrophotometer equipped with an ATR unit. Only relevant bands are quoted. FAB MS were recorded on a Thermo MAT95XP mass spectrometer, whereas ESI MS were recorded on a QStar Elite LC/MS mass spectrometer. NMR spectra were recorded at 298 K on a Varian Unity Inova 400 or on a Varian Inova 500 spectrometer. <sup>1</sup>H NMR chemical shifts were internally referenced to tetramethylsilane (TMS) via the residual <sup>1</sup>H DMSO-*d*<sub>6</sub> (δ = 2.50 ppm) according to the values reported by Fulmer et al. [60]. Chemical shift values are reported in parts per million and coupling

constants (J) are in Hertz. The splitting of proton resonances is defined as s = singlet, d = doublet, t = triplet, q = quadruplet, m = multiplet, bs = broad singlet. o, m and p stand for *ortho*, *meta* and *para*, respectively. 2D NMR spectra were recorded using standard pulse–pulse sequences: COrrrelation SpectroscopY (COSY), NuclearOverhauser Enhancement SpectroscopY (NOESY). The probe temperature ( $\pm 1$  K) was controlled by a standard unit calibrated with a methanol reference. All NMR data processing was performed using MestReNova version 6.0. Conductivity measurements were carried out with a CRISON 522 conductimeter, connected to a conductivity cell CRISON 52 92 with platinum electrodes. The solutions of the complexes ( $10^{-3}$  M, in acetonitrile) were prepared in 5 mL volumetric flasks and measured in test tubes.

### 2.2. X-ray diffraction studies.

X-ray structure determination was carried out for **6**·H<sub>2</sub>O, **7**·0.33(Me<sub>2</sub>CO) and **10**·Me<sub>2</sub>CO. Data were collected on a Bruker X8 APEX II CCD-based diffractometer, using a Mo-K $\alpha$  radiation source ( $\lambda = 0.71073$  Å). The raw data frames were integrated with the SAINT+ programme [61] using a narrow-frame integration algorithm. Corrections for Lorentz and polarization effects were also applied with SAINT+. The absorption correction was based on fitting a function to the empirical transmission surface as sampled by multiple equivalent measurements [62]. The structure was solved by a combination of direct methods and difference Fourier syntheses and refined by full-matrix least-squares on F2 with the WINGX software package [63,64]. All non-hydrogen atoms were refined with anisotropic thermal parameters. Hydrogen atoms were placed using a ‘riding model’ and included in the refinement at calculated positions. CCDC numbers for the new structures are the following: 2023022-2023024.

### 2.3. Cyclic Voltammetry.

CV Pt(IV) was performed on a potentiostat/galvanostat DropSens  $\mu$ Stat400 coupled to a Metrohm 757 VA Computrace cell at a potential sweep rate of 100 mV/s. A glassy carbon (GC) disk electrode (3 mm diameter) served as the working electrode, a coiled platinum wire was used as the counter electrode, and a Ag/AgCl (3M KCl) electrode was used as reference. Electrochemical measurements were performed in a 10 mL cell at an approximate complex

concentration of 10 mM using 0.1 M NaClO<sub>4</sub> in DMSO as supporting electrolyte. The samples were degassed by bubbling N<sub>2</sub> into the solution for 10 min before the voltammograms were recorded to ensure that they were oxygen-free. The GC electrode was polished with 0.05 μm γ-alumina slurry, rinsed clean with deionized water and ethanol, and subsequently dried. Each compound was obtained against its corresponding background, and all voltammograms were back-ground-corrected.

For standard reduction potentials (E<sup>0</sup>) determination, the same procedure described above was followed but a polished platinum disk electrode (3 mm diameter) was used as working electrode. Scan rates ranging from 0.01 to 1 V s<sup>-1</sup> were used and CVs were collected at different scan rates. Three CVs scan rate of 0.1 V s<sup>-1</sup> were carried out at the beginning, in the middle and at the end of the measurements series in order to check the reproducibility of the system. Overall, the peak potentials obtained at 0.1 V s<sup>-1</sup> did not change significantly (maximum uncertainty of ~19 mV). In each case the electrochemical transfer coefficient (α) and the effective or applied potential (E<sub>app</sub>) were calculated using the following equations.

$$\alpha = 0.5 + \frac{F}{2\lambda}(E_{app} - E^0)$$

$$\alpha = \frac{47.4}{\delta E_{pc}(mV)}$$

$$\delta E_{pc} = |E_{pc} - E_{pc/2}|$$

$$E_{app} = \left( \frac{E_{pc} + E_{pc/2}}{2} \right)$$

Where λ is the reorganization energy, δE<sub>pc</sub> is the voltammetric peak width and E<sub>pc/2</sub> is the potential at the half-height of the peak. The peak potential (E<sub>pc</sub>) was plotted against the logarithm of the scan rate (log ν) and the α value against E<sub>app</sub> (see Supporting Information) obtaining the corresponding standard reduction potential value, E<sup>0</sup>.

#### 2.4. UV-Visible spectroscopy.

Visible ultraviolet absorbance measurements were performed using a Secomam Uvikon XS spectrophotometer using the LabPower Junior program. Quartz cuvettes with 1 cm optical pitch

were used for the measurements. Matlab 2018b was used to adjust the experimental data to a by exponential data and obtain the hydrolysis constants.

### 2.5. Cytotoxicity assays.

Lung cancer cell line (A549) and colon cancer cell lines (HCT116 and HT-29) were purchased from ATCC (LCG Promochem). The breast cancer cell line MCF-7 was kindly provided by Dr. Alberto Ocaña (Translational Research Unit, Complejo Hospitalario Universitario de Albacete, Spain). Cells were maintained in a humidified incubator at 37°C in a 5% CO<sub>2</sub> atmosphere and subcultured 2–3 times a week with an appropriate plating density. Cells were grown in Dulbecco's Modified Eagle's medium supplemented with 10% heat inactivated fetal bovine serum, 1% glutamine plus antibiotics (Penicillin and Streptomycin). All cell culture reagents were provided by Lonza.

For dose-response assays,  $1 \times 10^4$  cells/well were seeded in 24-well plates. Twenty-four hours later, cells were treated at different concentrations of the compounds for 48 h and then, MTT assays were performed. The stock solutions for the different complexes were prepared at a concentration of 25 mM for DMSO and 6.25 mM for DMF. The corresponding volume of these solutions was taken to get the indicated final concentrations in the dose-response assays. The final concentration of DMSO/DMF in cell culture medium did not exceed 0.4%. Control cells were exposed to the maximum dose of solvent (DMF/DMSO 0,4% vol/vol) showing almost no toxicity (<6%) and used as 100% viability. Toxicity in dose-response assays was measured by using an MTT-based assay. Briefly, Thiazolyl Blue Tetrazolium Blue (MTT, Sigma-Aldrich) at 0.5 mg/ml in PBS (Phosphate Buffer Saline, pH 7,4) was added to the medium in each well at final concentration of 0.05 mg/ml and plates were incubated at 37 °C and 5% CO<sub>2</sub> for 1 h. Then, the medium-MTT was then removed and 500 µl DMSO were added to each well. Plates were kept in agitation for 5 min in the dark to dissolve the MTT-formazan crystals. The absorbance of the samples was then recorded at 570 nm in a Biochrom Asys UVM340 Microplate Reader. Data are the average of, at least, three independent experiments performed in triplicated cultures.

To calculate the IC<sub>50</sub> value, the decimal logarithm of the concentration is plotted against survival, and a non-linear regression is performed using a dose-response inhibition equation with

variable slope (four parameters) using the GraphPad Prism 6 software. The equation obtained has the following formula:

$$y = Bottom + \frac{(Top - Bottom)}{(1 + 10^{((LogIC50-x)*HillSlope)})}$$

The IC<sub>50</sub> value is obtained from LogIC<sub>50</sub>.

## 2.6. Stability/speciation studies

NMR studies: 8 mM solutions (DMSO-*d*<sub>6</sub>, DMF-*d*<sub>6</sub> or DMSO-*d*<sub>6</sub>/D<sub>2</sub>O 80/20) were prepared. <sup>1</sup>H-NMR spectra were recorded at different times to follow the appearance and disappearance of the different species.

Uv-vis studies: the uv-vis spectra of 10<sup>-5</sup> solutions of the complexes were registered at different times. For DMSO solutions, the spectra were collected every 2 min until 2 h, every 30 min until 7 hours and then, every 1.5 h until 24 h. For DMSO:H<sub>2</sub>O (5:95) solutions, the spectra were collected every 3 min until 1h, every 20 min until 4h 20 min and every 90 min up to 19h 20 min. The absorbance at the different times at the specified wavelengths was recorded.

## 2.7. Calculation of pK<sub>a</sub>.

Solution of the complexes at 10<sup>-5</sup> M in the DMSO/H<sub>2</sub>O (80/20) mixture with Bu<sub>4</sub>NBF<sub>4</sub> at 5mM were studied by UV-vis. Evolution of the peaks were studied at different pH. Aliquots of 10 μL of HCl (0.002M) or 10 μL of NaOH (0.002M) were added to a solution of 2 mL of complexes **9** and **13**, to vary the pH. The absorbance spectrum was recorded after that.

The absorbance versus pH plot (Figures S47 y S48) enables to determine one constant according to equation from the Wilson and Lester method:[65]

$$\log K = \log \frac{Am - Aa}{Ab - Am} + pH$$

where Aa is the absorbance for the acid species, Ab is the absorbance for the basic species and Am is the absorbance of the mixture. Representing log(Am-Aa)/(Ab-Am) versus pH, the intersection will provide the pK<sub>a</sub> value; when log(Am-Aa)/(Ab-Am) is equal to zero, the pK<sub>a</sub> equals to pH.

### 2.8. *Electrophoretic Mobility in Agarose Gel.*

The pUC18 plasmid DNA was used at a concentration of 0.5  $\mu\text{g}/\mu\text{L}$  (1512  $\mu\text{M}$  nucleotides; 756  $\mu\text{M}$  bp). Complex stock solutions at 500  $\mu\text{M}$  were freshly prepared in Milli-Q from a 10 mM solution of the complex in DMSO to facilitate the dissolution of the compound, giving a 5 % of DMSO in the stock solutions. Reactions were performed by mixing 0.5  $\mu\text{L}$  of pUC18 with appropriate aliquots of complex solutions. Tris-EDTA (TE) (Tris-H<sub>4</sub>edta, tris(hydroxymethyl)aminomethane ethylenediaminetetracetic acid) buffer solution (50 mM NaCl, 10 mM Tris-HCl, 0.1 mM H<sub>4</sub>edta, pH 7.4) was added to the mixture to give a final volume of 20  $\mu\text{L}$ . The maximum percentage of DMSO was 2% for the most concentrated solution used, 200  $\mu\text{M}$ . The final concentration of pUC18 DNA was 37.8  $\mu\text{M}$  in nucleotides (18.9  $\mu\text{M}$  bp). The samples were incubated at 37 °C for 16 hours. The reactions were quenched by adding a buffer solution (4  $\mu\text{L}$ ) consisting of bromo-phenol blue (0.25%), xylene cyanole (0.25%), and glycerol (30%). The samples were then subjected to electrophoresis on 0.8% agarose gel in 0.5  $\times$  TBE buffer (0.045 M Tris, 0.045 M boric acid, and 1 mM EDTA) at 100 V for 1 h 40 min. Finally, the DNA was dyed with an ethidium bromide solution (10 mg/mL in TBE) for 15 min and the DNA bands were visualized on a capturing system (ProgRes CapturePro 2.7). Samples of Pt(IV) complexes were treated as described above but adding 2.25  $\mu\text{L}$  of 2 mM ascorbate.

### 2.9. *Flow cytometry.*

For apoptosis detection,  $2 \cdot 10^5$  cells were seeded in 6 cm plates, 24 h later cells were treated for 24 h with the indicated amounts of each compound and then trypsinized. Next, cells were washed with PBS and resuspended in Annexin V Binding Buffer (Immunostep). The cells were then incubated with Annexin V-FITC (Immunostep) for 20 min in dark and then incubated with 10  $\mu\text{g}/\text{ml}$  propidium iodide (PI) and 20  $\mu\text{g}/\text{ml}$  RNase for 10 min in dark. Samples were analysed in a MACSQuant Analyzer 10 (Miltenyi Biotec). Data were analysed by using FlowingSoftware (University of Turku).

### 2.10. *Haemolytic activity.*

The haemolytic activity of the compounds was evaluated by determining haemoglobin release from erythrocyte suspensions. To this end, swine blood was freshly obtained and diluted

5% v/v in PBS. Blood was centrifuged at 1000 rcf for 10 minutes, washed three times with PBS and resuspended in PBS to reconstitute the starting volume. Subsequently, 150  $\mu$ L of red blood cells suspension were mixed with 150  $\mu$ L of each compound at different concentrations (5, 10, 25 and 50  $\mu$ M). A solution of 2% Triton X-1000 in PBS was used as positive control to achieve complete haemolysis. PBS alone was used as negative control. Samples were incubated for 1h at 37 °C under continuous shaking (50 rpm) and then centrifuged at 3500 rcf for 10 minutes. Eighty microliters aliquots of the supernatant were transferred to a 96-well plate and diluted with Milli-Q 80  $\mu$ L of water. Haemolysis was evaluated by measuring the absorbance of the samples at 540 nm with a plate reader (BioTek, Winooski, USA). The percentage of haemolysis (H) was calculated using the equation:  $H=100 [(A_s-A_n) / (A_p-A_n)]$ , where  $A_s$  was the absorbance for a given sample,  $A_n$  for the negative control and  $A_p$  for the positive control. Each sample was tested by triplicate.

#### 2.11. Cellular uptake studies.

To assess the cellular internalization of compounds **7**, **8**, **13** and **14**,  $2 \times 10^6$  MCF7 cells were plated in 60 mm Petri dishes and allowed to attach for 24 h. The plates were then exposed to the compounds at a concentration equivalent to the IC<sub>50</sub> value of the Pt(II) congener (5  $\mu$ M for **7** and **8** and 2  $\mu$ M for **13** and **14**). Cisplatin was included at the same concentrations as a positive control. Additional plates were incubated with medium alone as negative control. All treatments were conducted in triplicate. After 3 h of incubation, cells were washed three times with cold PBS and harvested by trypsinisation. The cells were then centrifuged to obtain the whole cell pellet. The platinum content inside the cell was next determined by ICP-MS analysis. To this end, the cell pellets were dissolved in 400  $\mu$ L of 69% v/v nitric acid (PanReac Applichem) and heated in a water bath at 100 °C for 18 h. Samples were then allowed to cool and diluted with Milli-Q water to a final volume of 10 mL. Platinum content was analysed on an ICP-MS Agilent 7500c instrument at the Serveis Tècnics de Recerca de la Universitat de Girona. The platinum standards were freshly prepared from a platinum atomic absorption standard solution at 1000 ppm Pt in 5% HCl (Aldrich) diluted in Milli-Q water with 2% HNO<sub>3</sub>. The concentrations used for the calibration curve were 0, 0.2, 0.4, 1, 2, 5 and 10 ppb. Three isotopes were analysed (<sup>194</sup>Pt – <sup>195</sup>Pt – <sup>196</sup>Pt) and

all readings were made in triplicate. Rhodium was added as an internal standard at a concentration of 100 ppb in all samples.

### 2.12. Quantum chemical calculations.

The software package Gaussian 09 [66] (see full reference in SI) was employed to perform all the calculations. The structures of complexes **13** and **14** were optimised by DFT calculations. For the aquation studies, the geometries of molecules and transition states (TS) were optimised using the functional B3LYP [67,68] and to obtain better descriptions, D3 Grimme dispersion was added with the Becke–Johnson damping, including ‘ultrafine integration grid’ implemented in Gaussian 09 [69].

The Pt atom was described using LAN2DZ[70] complemented with a set *f* polarization function [71]. The 6-31G(d,p) basis set was used for the other elements [72]. The structures of the reactants, intermediates, transition states and products were optimised in water solvent ( $\epsilon = 78.35$ ) using the cluster-continuum model (SMD) [73]. Frequency calculations were carried out for all of the optimised geometries to characterise the stationary points (zero imaginary frequency) as either minima or transition states (one imaginary frequency). Intrinsic reaction coordinate (IRC) calculations were carried out for the transition states to confirm that they connected with the corresponding structures [74]. All energies collected in the text are Gibbs energies in water at 298 K.

Single point calculations with the large basis set 6-311++G (d, p) for the C, H, O, N, Cl atoms and LAN2DZ+*f* for Pt, using previously optimised geometries, were performed in order to obtain more accurate relative energies. Potential energy profiles were estimated from total electronic energy at the 6-311++G (d, p) level and adding the enthalpy corrections at the standard state, at 298.15 K and 1 atm. The rate constants (*k*) for each step were calculated according to Eyring’s equation [75].

$$k(T) = \left( \frac{K_B T}{h} \right) e^{\Delta G^\ddagger / RT}$$

T is the absolute temperature and  $K_B$ , h, and  $\Delta G^\ddagger$  are the Boltzmann constant, Planck constant and the free energy of activation of each step, respectively. All calculations were performed at standard concentrations ( $c^0 = 1 \text{ mol/dm}^3$ ).

In an effort to explain the photophysical properties of **13** the lowest-lying singlets ( $S_n$ ) were computed using the Time-Dependent Density Functional Theory (TD-DFT) approach[76] at the B3LYP-D3/6-31G(d,p)/LANL2DZ level of theory. These calculations were performed on the minimum-energy geometry previously optimised for  $S_0$  in acetonitrile as solvent ( $\epsilon = 37.5$ ).

### 2.13. *Synthesis and characterisation of the new complexes.*

This aspect is included in the Supporting Information.

## 3. Results and Discussion

### 3.1. *Synthesis and general characterisation.*

Ligands **L1**, **L4**, **L5** and **L7** were commercially available, whereas **L2** [58] and **L3** [59] were prepared by previously reported methods. The synthesis of **L6** is described for the first time in this work and the same synthetic methodology was used as for **L2–L3**.

Complexes **1–14** (see Figure 2) were synthesised as indicated in Scheme 1. Compounds **1** [77–81], **7** [79] and **9** [82] and were previously described but were synthesised in this work in order to obtain structure-activity relationships (SAR) with other complexes and to compare their behaviour with that of their Pt(IV) analogues. The cytotoxic activities of complexes **1** [77,78,81] and **9** [82] were studied and they were found to be active against several cell lines. We previously reported the synthesis of **5** [59], which showed cytotoxic activity against HeLa and serum-deprived A549 cell lines.

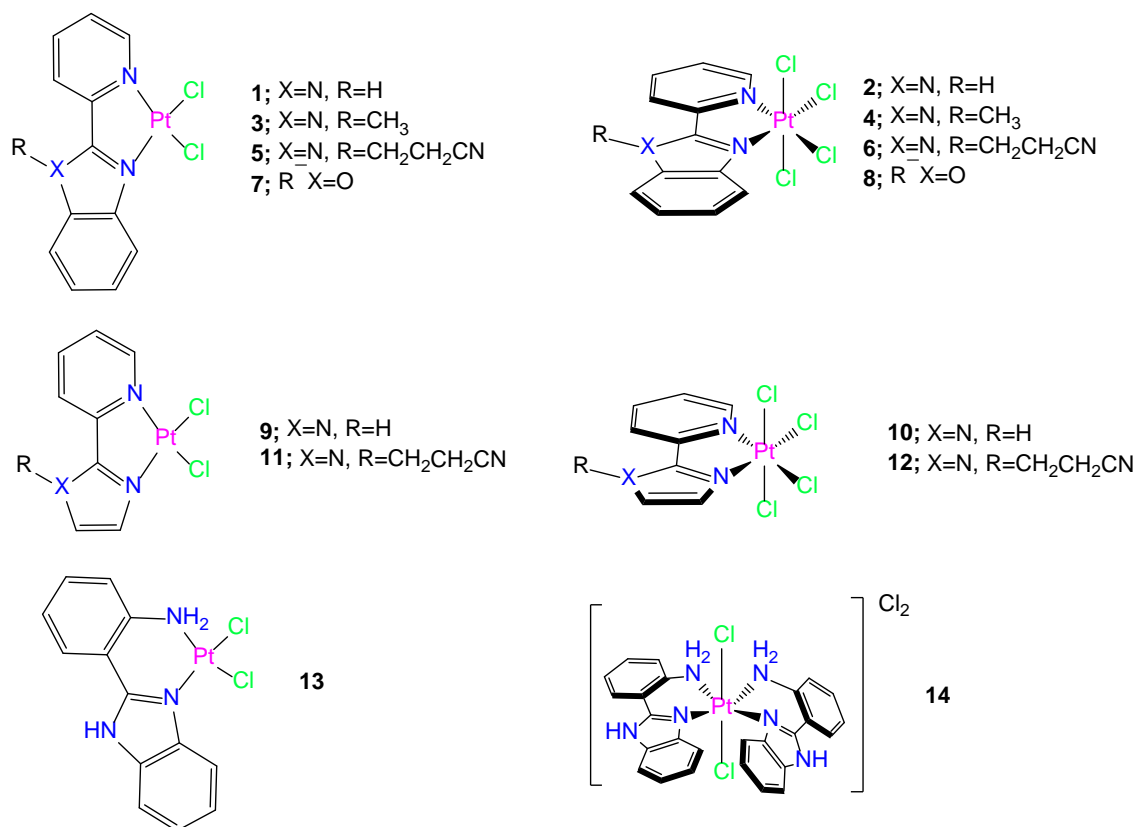
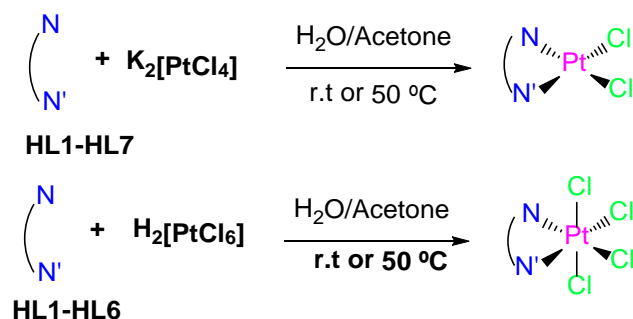


**Figure 2:** Pt(II) and Pt(IV) compounds synthesised in this work.

Oxidation with Cl<sub>2</sub> or H<sub>2</sub>O<sub>2</sub> of the corresponding Pt(II) precursors is the most common method to obtain anticancer Pt(IV) derivatives that can be further derivatized [83], but in this case the formulation of the target Pt(IV) complexes prevented the use of this oxidation step. It has been reported that complexes of the type [Pt(L<sup>Λ</sup>L)Cl<sub>4</sub>], where L<sup>Λ</sup>L is a chelating diamine ligand, can be synthesised by the reaction of the sodium or potassium salts of the [PtCl<sub>6</sub>]<sup>2-</sup> anion with L<sup>Λ</sup>L in water, usually under reflux [83–88]. The procedure was modified by using H<sub>2</sub>[PtCl<sub>6</sub>].6H<sub>2</sub>O as the precursor, which facilitates the solubility of the ligand in the acetone/water mixtures used and the reactions were performed under mild conditions at room temperature or 50 °C. In the case of **L7**, the resulting platinum(IV) compound, **14**, contained two coordinated chelate ligands [PtCl<sub>2</sub>(**L7**)<sub>2</sub>]Cl<sub>2</sub>. This compound was formed on using equimolar quantities of ligand and H<sub>2</sub>[PtCl<sub>6</sub>] or even with an excess of the platinum precursor. The 1:2 electrolyte character was verified by measuring the conductivity [89]. The value obtained was 193.6 S. cm<sup>2</sup>.mol<sup>-1</sup>. This complex can exist as four possible isomers (see Figure 3). DFT calculations were carried out to

determine that the most stable isomer is that with the chloride ligands in a trans arrangement and the similar fragments of the bidentate ligand in a cis orientation.



**Scheme 1:** Synthesis of Pt(II) and Pt(IV) complexes.

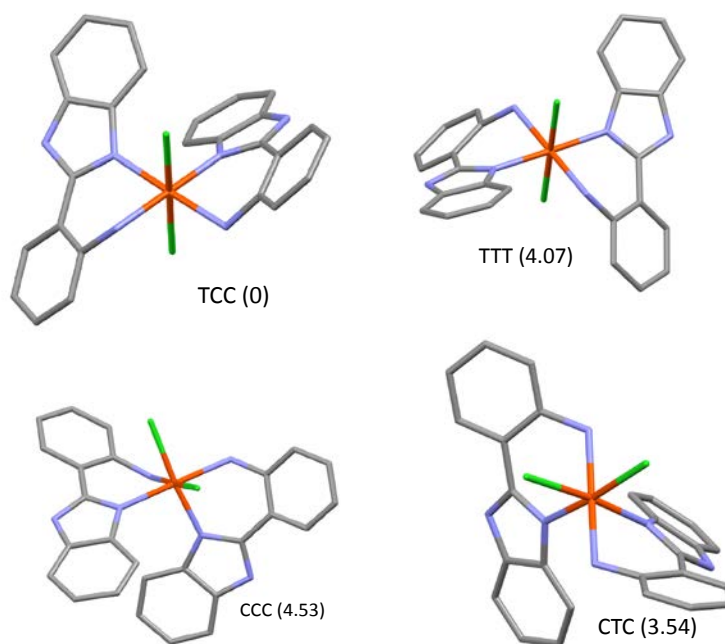
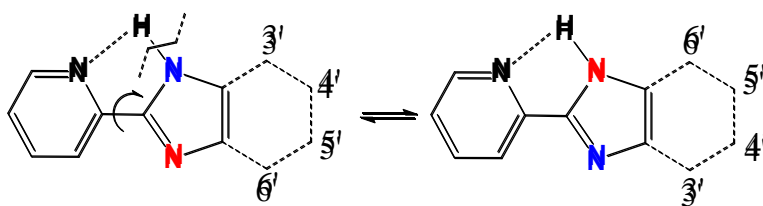


**Figure 3.** Possible isomers of complex **14** and the corresponding  $\Delta G(\text{kcal/mol})$  relative values, calculated by DFT studies. (T = trans, C = cis, the order used to specify the relative arrangement of the ligands is chloride, aniline and benzimidazole fragments of the chelate ligand). H atoms have been omitted for clarity.

All of the complexes were isolated as brown, orange or yellow solids in moderate-to-good yields. All of the complexes are soluble in DMSO and moderately soluble in the DMSO/H<sub>2</sub>O mixtures used in the biological studies, with the exception of compounds **3** and **4**, for which the

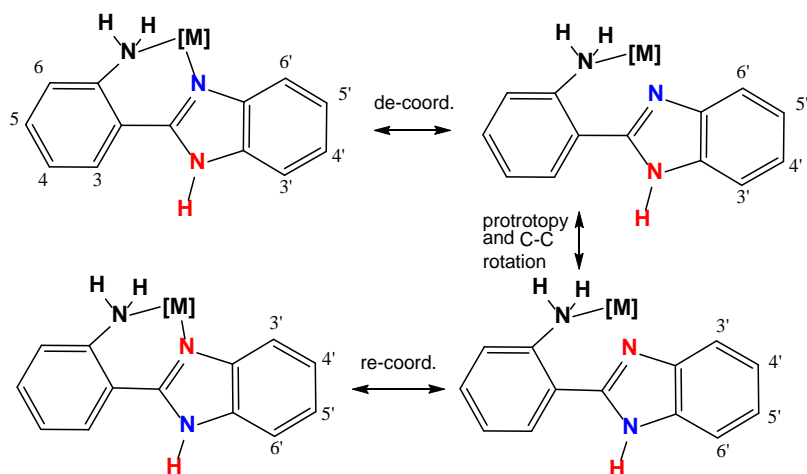
lack of solubility in DMSO and DMSO/H<sub>2</sub>O mixtures made it impossible to study their biological properties. Ligands and complexes were characterised by NMR and IR spectroscopies. Fast atom bombardment (FAB<sup>+</sup>) and Electrospray ionization (ESI) mass spectra for the complexes were also recorded. The peaks observed are consistent with the proposed formulations. [M – Cl + DMSO]<sup>+</sup> or [M + Na]<sup>+</sup> peaks were observed in the FAB<sup>+</sup> and ESI spectra, respectively (see Experimental Section, in SI). The assignment of the NMR resonances was facilitated by two-dimensional experiments such as gCOSY and NOESY. As one would expect, the coordination of the ligands caused deshielding in the <sup>1</sup>H-NMR resonances of the protons of the coordinated rings. The effect was more marked for the protons adjacent to the N-donor atoms (see Experimental Section and Tables S1–S2, where the data for the ligands are also included). In general, the resonances of the Pt(IV) complexes appear at lower fields than those of their Pt(II) counterparts. The effect is more marked in the pairs **5/6**, **9/10** and **11/12**. <sup>195</sup>Pt-<sup>1</sup>H coupling satellites were observed in the signals corresponding to CH protons adjacent to the coordination sites (<sup>3</sup>J<sub>Pt-H</sub> = 26–28.5 Hz and 8–11 Hz for the pyridine and imidazolyl rings, respectively). In complex **14**, this coupling in the amino resonance was not observed, probably due to the broadening of the signal. The <sup>195</sup>Pt-<sup>1</sup>H coupling could not be observed in their Pt(II) analogues. This fact has been previously reported and is attributed to the presence of larger <sup>1</sup>J<sub>Pt-N</sub> values (often hundreds of Hz) in Pt(II) complexes, which may, along with sizeable <sup>14</sup>N relaxation rates, cause a more severe shortening of T2 (<sup>195</sup>Pt) [90].

It is interesting to analyse the resonances of ligands **L1**, **L5** and **L7**, in which prototropy processes are possible (see Scheme 2) and compare them with those of the corresponding platinum complexes, with special attention paid to complex **14** as it has a different stoichiometry. In the three ligands this interchange process may be restricted by the formation of hydrogen bonds. In fact, in ligands **L1** and **L5** broad resonances are observed for the benzimidazolyl (**L1**, H<sup>3'</sup> and H<sup>6'</sup> broad resonances, H<sup>4'</sup> and H<sup>5'</sup> same multiplet) or imidazolyl (**L5**, broad signal for H<sup>4'</sup>+H<sup>5'</sup>) rings and this reflects a dynamic process, although the situation of fast interchange is not reached. When the ligands are coordinated, the resonances are all narrow and this indicates that the prototropy process has been arrested and shows the asymmetry of the corresponding rings.



Scheme 2. Prototropy process for ligands **L1** and **L5**.

The situation for **L7** and its Pt complexes is different (see Figure S1). Firstly, in the ligand all of the signals of the benzimidazole fragment are narrow and different, which shows the absence of prototropy, probably due to the formation of a hydrogen bond with the amino group that is stronger than that found in **L1** or **L5**. If we define  $\Delta\delta = \delta_{\text{complex}} - \delta_{\text{ligand}}$ , in the case of complex **13** the highest values (positive) are observed for  $\text{NH}_2$ ,  $\text{H}^5$ ,  $\text{H}^6$  and  $\text{H}^{6'}$  ( $\Delta\delta = 0.7\text{--}0.8$  ppm, see Scheme 3 for atom numbering of the ligand), an effect that should be due to coordination to the metal fragment. In the case of **14**, the  $\Delta\delta$  values are generally smaller, and this indicates a possible weaker coordination and a significant difference with respect **13** is observed: all resonances of the benzimidazole ring are broad and even the protons  $\text{H}^5$  and  $\text{H}^{4'}$  appear together in the same broad signal (see Figure S1). This observation can be explained by a dynamic process of partial de-coordination of the N atom of the benzimidazole fragment, which is thought to be caused by the higher steric hindrance in **14** due to the presence of two ligands in the octahedral environment. The rotation around the C(aniline)–C(benzimidazole) bond accompanied by prototropy and re-coordination of the other N atom should interconvert  $\text{H}^{6'}$  with  $\text{H}^{3'}$  and  $\text{H}^{4'}$  with  $\text{H}^{5'}$  (see Scheme 3). This prototropy can take place in the case of **14** because the amino group is involved in the coordination to the metal centre.



Scheme 3. Proposed dynamic process for the interconversion of the benzimidazole protons of a [M]-L7 fragment in **14**. The atom numbering is shown.

### 3.2. X-ray diffraction studies.

Single crystals of complexes **6.H<sub>2</sub>O**, **7.(Me<sub>2</sub>CO)<sub>0.33</sub>** and **10.Me<sub>2</sub>CO** suitable for X-ray diffraction analysis were obtained by recrystallisation from DMSO (for complex **6**) or by slow diffusion of an acetone solution of the corresponding ligand to an aqueous solution of the platinum precursor. The crystal data are provided in Table S3 and selected coordination distances are gathered in Table 1. The ORTEP representation of the Pt(II) complex **7** is shown in Figure 4 and those of the Pt(IV) complexes **6** and **10** are shown in Figure 5. In the case of **7**, there are three independent molecules in the unit cell and, as one would expect, the geometry around the Pt(II) centre is square planar. The  $\tau_4$ [91] value is 0.05 or 0.07 depending on the molecule and therefore the geometry is only slightly distorted. An octahedral geometry was found for the Pt(IV) complexes. The bite angle in **7** has values of 81.1°, 80.6° and 80.6° while this angle is slightly smaller for **6** (79.7°) and **10** (79.9°). The ligands are essentially planar and the dihedral angles between the pyridine ring and the other fragment of the ligand are 3.1–4.6° for **7**, 2.9° for **10** and a value higher (6.4°) for **6**. The Pt–N and Pt–Cl distances are in the expected range according to the bibliography [80,87,88,92–95]. In the case of the two Pt(IV) complexes, the Pt–Cl distances are slightly longer when the chloride ligand is trans to another chloride than when it is trans to an N-donor fragment. The marked variation in the Pt–Cl and Pt–N(benzoxazole) distances in the three molecules of **7** is worth highlighting and this shows a significant contribution of the weak

interactions in the crystal. Concerning the Pt–N distances of a given complex, a slightly higher value is found for the Pt–N(pyridine) bond.

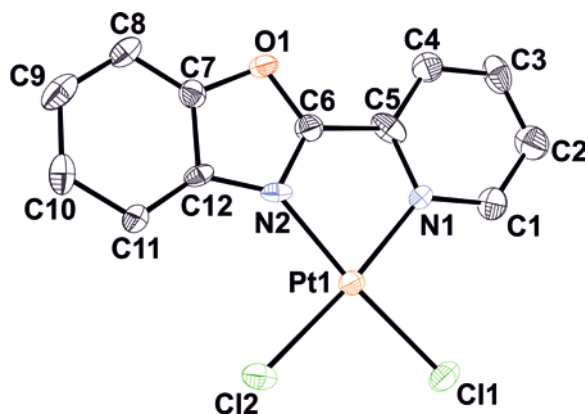


**Figure 4:** ORTEP diagram of complex **7** (molecule containing Pt1). H atoms and solvent molecules have been omitted.

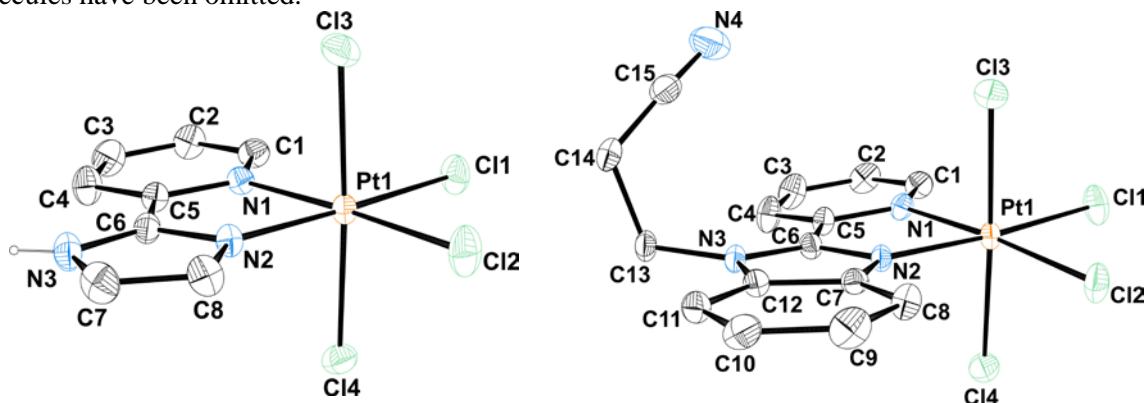


**Figure 5:** ORTEP diagrams of complexes **10** (left) and **6** (right). H atoms, except that of the NH group in **10**, and solvent molecules have been omitted.

**Table 1**

Pt–Cl and Pt–N bond distances of compounds **10**.Me<sub>2</sub>CO, **7**.(Me<sub>2</sub>CO)<sub>0.33</sub> and **6**.H<sub>2</sub>O.

Complex	Bond	Distance (Å)
<b>7</b> .(Me <sub>2</sub> CO) <sub>0.33</sub>	Pt(1)-N(2)	2.04(1)
	Pt(2)-N(4)	2.02(1)
	Pt(3)-N(6)	2.00(1)
<b>10</b> .Me <sub>2</sub> CO	Pt(1)-N(1)	2.02(1)
	Pt(2)-N(3)	2.03(1)
	Pt(3)-N(5)	2.03(1)
<b>6</b> .H <sub>2</sub> O	Pt(1)-Cl(2)	2.313(5)
	Pt(2)-Cl(4)	2.87(4)

	Pt(3)-Cl(6)	2.298(4)
	Pt(1)-Cl(1)	2.289(4)
	Pt(2)-Cl(3)	2.291(4)
	Pt(3)-Cl(5)	2.297(4)
<b>6.H<sub>2</sub>O</b>	Pt(1)-N(1)	2.053(3)
	Pt(1)-N(2)	2.016(3)
	Pt(1)-Cl(2)	2.293(1)
	Pt(1)-Cl(1)	2.294(1)
	Pt(1)-Cl(3)	2.308(1)
	Pt(1)-Cl(4)	2.311(1)
<b>10.Me<sub>2</sub>CO</b>	Pt(1)-N(2)	2.002(3)
	Pt(1)-N(1)	2.046(3)
	Pt(1)-Cl(3)	2.304(1)
	Pt(1)-Cl(2)	2.289(1)
	Pt(1)-Cl(4)	2.309(1)
	Pt(1)-Cl(1)	2.300(1)

As far as the 3D structure is concerned, in the case of complex **7.(Me<sub>2</sub>CO)<sub>0.33</sub>** columns of stacked molecules are formed that extend along the *a* axis and this follows the order Pt1...Pt2...Pt3...Pt1...Pt2.... There are Pt1...Pt2 and Pt2...Pt3 contacts and  $\pi$ - $\pi$  stacking interactions (double in the case of the contact between molecules with Pt1 and Pt3) involving the benzoxazole moieties (for further details see Figure S2 and Table S4). The interactions between columns take place through hydrogen bonds involving chloride ligands, acetone molecules and O2 of a benzoxazole ring (see Figure S3). There are also lone pair- $\pi$  interactions between some chloride ligands and oxazole or pyridine rings. In the 3D crystal structure of **6.H<sub>2</sub>O**, chains of molecules that extend along the *b* axis are also observed. In these chains two types of loop alternate (Figure S4). One loop is formed by two hydrogen bonds that involve a chloride ligand and two equivalent  $\pi$ - $\pi$  stacking interactions of the benzimidazole unit that is arranged in a head-to tail fashion. In the formation of the other loop, hydrogen bonds that involve the N atom of the CN group participate along with a  $\pi$ - $\pi$  stacking interaction between two pyridine rings (Table

S4). The 3D structure is shaped by the direct interaction of the chains through hydrogen bonds with the participation of chloride ligands and also with the participation of the water solvent molecules (Figure S5). In the case of complex **10.Me<sub>2</sub>CO**,  $\pi$ - $\pi$  stacking interactions are also observed and columns are formed along the *c* axis, with stacking between pairs of pyridine rings of two ligands and also between pairs of imidazolyl rings. The ligands of adjacent molecules are oriented in a head-to-tail manner (see Figure S6 and Table S4). In the 3D structure, hydrogen bonds involving the complexes and the acetone molecules are observed and Cl $\cdots$ Cl interactions [96] are also formed (see Figure S7).

### 3.3. Electrochemical studies.

The redox potentials of complexes **1–12** were measured (10 mM DMSO solutions) by cyclic voltammetry. Complexes **3** and **4** could not be studied due to their poor solubility in the medium. The potential corresponding to the reduction of the Pt(IV) centre (Table 2) was found by comparing the cyclic voltammograms of the Pt(IV) complexes with those of their Pt(II) analogues, as an irreversible peak is found in the former but not in the latter (see Supporting Information, Figures S8–S13). The rest of the peaks were assigned as ligand redox processes [51].

**Table 2.**

Peak reduction potentials of the complexes in DMSO solution vs Ag/AgCl. In bold, reduction potentials assigned to the reduction of the Pt(IV) centre.

Comp.	Peak reduction potential (V)
<b>1</b>	-0.03 (r), -1.5 (r)
<b>2</b>	0.03(r), <b>-0.43</b> (ir), -1.34 (ir)
<b>5</b>	-0.98 (ir), -1.27(r)
<b>6</b>	<b>-0.31</b> (ir), -1.01(ir), -1.25 (r)
<b>7</b>	-1.03 (r)
<b>8</b>	<b>-0.15</b> (ir), -1.05 (r)
<b>9</b>	0.01 (r), -1.36 (ir)
<b>10</b>	0.03 (r), <b>-0.37</b> (ir), -1.3 (ir)
<b>11</b>	-1.2 (ir), -1.5 (ir)

<b>12</b>	<b>-0.33</b> (ir), -1.2 (ir), -1.52(r)
<b>13</b>	0.01(r), -1.43 (ir)
<b>14</b>	-0.1 (r) <b>-0.67</b> (ir), -1.38 (ir)

---

### *3.4. Electronic spectra and TD-DFT analysis of 13.*

Considering that complex **13** is the most interesting compound in terms of the biological properties (see below), it was decided to characterise this compound in more detail by recording the ultraviolet-visible (UV-vis) absorption spectrum (acetonitrile solution, room temperature, see Figure S14). Time-Dependent Density Functional Theory (TD-DFT) was applied in an effort to understand the nature of the electronic transition.

The theoretically calculated electronic transition of **13** was found at 305 nm, which is in good agreement with the experimental value of  $\lambda_{\text{max}}$  at 299 nm (Figure S14).

The isovalue contour plots of some frontier orbitals are presented in Figure 6 along with the energy levels (see Table S5 for the energy of a selection of molecular orbitals). The HOMO-LUMO energy gap is 4.25 eV.

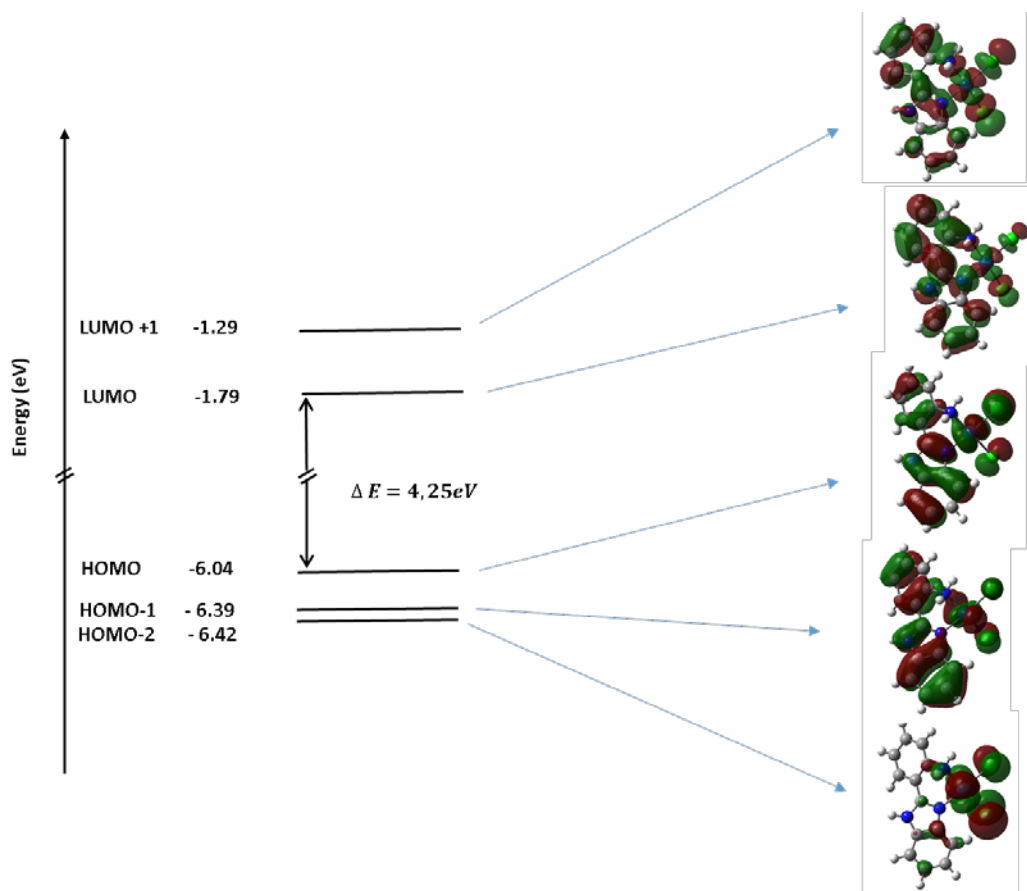


**Figure 6.** Energy (eV) and contours of some frontier molecular orbitals of complex **13** in acetonitrile. See Experimental Section for details.

The assignments of the calculated transitions to the experimental bands (summarised in Table 3) are based on the criteria that the oscillator strengths and the orbital contributions are greater than 0.01 and 10%, respectively. The TD-DFT calculated excited singlet states that show a better fit with the experimental values of 299 nm are  $S_6$  and  $S_7$ , which display predicted energies of 4.06 eV (305 nm) and 4.10 eV (302 nm), respectively. Both states are mainly defined by transitions from the HOMO-1 to LUMO (48% in  $S_6$  and 28% in  $S_7$ ) and HOMO-2 to LUMO (24% in  $S_6$  and 25% in  $S_7$ ) (see Table S6 for the single states  $S_1$ – $S_4$  and Table S7 for the calculated contributions of the atomic orbitals in the frontier molecular orbitals). In the case of  $S_7$  there is also a contribution (38%) of a transition from the HOMO-2 to LUMO+1. The HOMO-1 to LUMO can be described as a metal-to-ligand charge transfer ( $^1\text{MLCT}$ ) transition because of the reduction in the participation of the orbitals of the platinum in the LUMO when compared with the HOMO-1 (see Table S7). In addition, this transition shows some metal-centred ( $^1\text{MC}$ ) character due to the

different atomic orbitals of the platinum atom involved in these two molecular orbitals, and this transition also displays ligand-centred (<sup>1</sup>LC) character because of the different natures of the orbitals belonging to the N-donor ligand ( $\pi$ -bonding in HOMO-1 and  $\pi^*$  in LUMO). The transition HOMO-2 to LUMO can be described as a metal-to-ligand charge transfer (<sup>1</sup>MLCT) because of the reduction in the participation of the orbitals of the platinum in the LUMO when compared with HOMO-2 (see Table S7). For a similar reason, this transition can also be described as a ligand-to-ligand charge transfer (<sup>1</sup>LLCT) from a p orbital of the chloride ligand labelled as Cl3 to a  $\pi^*$  molecular orbital of the N-donor ligand. The transition HOMO-2 to LUMO+1 found in S<sub>7</sub> shows a metal-centred (<sup>1</sup>MC) nature due to the different atomic orbitals of the platinum atom involved in these molecular orbitals. This transition also shows some metal-to-ligand charge transfer (<sup>1</sup>MLCT) and a ligand-to-ligand charge transfer (<sup>1</sup>LLCT) from a p orbital of the chloride ligand labelled as Cl3 to a  $\pi^*$  molecular orbital of the N-donor ligand.

**Table 3**

Vertical excitation energies for lower excited states calculated at TD-DFT B3LYP-D3 (6-31G\*\* / LANL2Dz+f) in acetonitrile solution.

State	E(eV,nm)/ f	Monoexcitations	Nature	Description
S <sub>5</sub>	3.86; 321,35/0.145	H → L (51%)	$d_{\pi}(\text{Pt}) + \pi_{L7} + p_{\text{Cl}} \rightarrow$ $d_{\pi}(\text{Pt}) + \pi^*_{L7}$	<sup>1</sup> MC, <sup>1</sup> LC, <sup>1</sup> LLCT, <sup>1</sup> MLCT
		H → L+1 (42%)	$d_{\pi}(\text{Pt}) + \pi_{L7} + p_{\text{Cl}} \rightarrow$ $d_{\pi}(\text{Pt}) + \pi^*_{L7} + p_{\text{Cl}}$	<sup>1</sup> MC, <sup>1</sup> LC, <sup>1</sup> LLCT
S <sub>6</sub>	4.06; 305,19/ 0.183	H-2 → L (24%)	$d_{\pi}(\text{Pt}) + p_{\text{Cl}} \rightarrow$ $d_{\pi}(\text{Pt}) + \pi^*_{L7}$	<sup>1</sup> MC, <sup>1</sup> LLCT
		H-1 → L (48%)	$d_{\pi}(\text{Pt}) + \pi_{L7} \rightarrow$ $d_{\pi}(\text{Pt}) + \pi^*_{L7}$	<sup>1</sup> MC, <sup>1</sup> LC, <sup>1</sup> MLCT
S <sub>7</sub>	4.10; 302, 12/ 0.048	H-2 → L (25%)	$d_{\pi}(\text{Pt}) + p_{\text{Cl}} \rightarrow$ $d_{\pi}(\text{Pt}) + \pi^*_{L7}$	<sup>1</sup> MC, <sup>1</sup> LLCT, <sup>1</sup> MLCT
		H-2 → L+1 (38%)	$d_{\pi}(\text{Pt}) + p_{\text{Cl}} \rightarrow$ $d_{\pi}(\text{Pt}) + \pi^*_{L7} + p_{\text{Cl}}$	<sup>1</sup> MC, <sup>1</sup> LC, <sup>1</sup> MLCT, <sup>1</sup> LLCT
		H-1 → L (28%)	$d_{\pi}(\text{Pt}) + \pi_{L7} \rightarrow$ $d_{\pi}(\text{Pt}) + \pi^*_{L7}$	<sup>1</sup> MC, <sup>1</sup> LC, <sup>1</sup> MLCT

### 3.5. Cytotoxicity.

The cytotoxicity of all of the compounds was studied in human lung carcinoma (A549), human breast carcinoma (MCF7) and human colon carcinoma (HCT116 and HT29) cell lines. The maximum concentration used in the studies was 25  $\mu\text{M}$  and the incubation time was 48 h.

Three Pt(II) compounds (**7**, **9** and **13**) and only one Pt(IV) compound (**10**) showed cytotoxicity in the studied cell lines with the concentration limit of 25  $\mu$ M. The half maximal inhibitory concentration ( $IC_{50}$ ) values are summarised in Table 4 (see Figures S15–S18).

**Table 4**

$IC_{50}$  values ( $\mu$ M) of compounds **7**, **9**, **10**, and **13** in different tumoral cell lines (48 h incubation time).

Compound	A549	MCF7	HCT116	HT29
<b>7</b>	>25	4.82 $\pm$ 1.25	1.29 $\pm$ 0.28	8.3 $\pm$ 4.7
<b>9</b>	> 25	> 25	13.9 $\pm$ 1.4	12.1 $\pm$ 1.7
<b>10</b>	> 25	> 25	16.5 $\pm$ 0.6	> 25
<b>13</b>	<2	1.99 $\pm$ 0.99	1.25 $\pm$ 0.18	2.1 $\pm$ 0.5
<b>Cisplatin</b>	16.30 $\pm$ 3.79	16.74 $\pm$ 2.23	15.36 $\pm$ 4.76	18.93 $\pm$ 3.19

Complex **9** has a slightly better cytotoxicity than cisplatin in colon cell lines (HCT116 and HT29), with values of  $IC_{50}$  > 25 in the rest of the studied cell lines. The cytotoxicity of **7** is quite high in all cell lines except for A549, with  $IC_{50}$  values lower than 10  $\mu$ M. The best results were obtained with **13**, which killed 50% of the cell population at less than 2  $\mu$ M in all cell lines. It is noteworthy that complex **13** is the only complex (apart from cisplatin) that is active in the A549 cell line. Thus, it can be concluded that in the case of complexes with ligands containing a pyridine fragment, the most cytotoxic compound is that with a benzoxazole unit but the most notable increase in the cytotoxic behaviour is achieved when the aniline fragment is present in the N<sup>^</sup>N' ligand. Cytotoxicity relatively similar to that of cisplatin has been previously found in platinum complexes with monodentate aniline derived ligands [97,98] and, as stated in the introduction, it has been described a dichloride platinum complex with a bidentate 2(amino-methyl)aniline ligand with high cytotoxicity [57] but complex **13** exhibits better performance.

As far as the Pt(IV) derivatives are concerned, only compound **10** showed a cytotoxicity similar to that of its Pt(II) analogue in the HCT116 line, which means that it is reduced inside the cells but, curiously, this is not the case for the HT29 cell line ( $IC_{50}$  > 25). In contrast to **10**, Pt(IV) compounds **8** and **14** do not have the same cytotoxicity than their Pt(II) analogues and in fact, are

not cytotoxic in the concentration limit studied. Thus, taking account of the results reported in the literature with other axial ligands [29,31,43], compounds with formula  $[\text{PtCl}_4(\text{N}^{\wedge}\text{N}^{\prime})]$  are not the best candidates for Pt(IV) prodrugs.

Considering a previous work [99] where a deleterious effect of the DMSO solvent in the cytotoxicity of several Pt(II) complexes and the influence of DMSO observed in complexes with other metals were described [100], we decided to test the cytotoxicity using DMF instead of DMSO for the active compounds and the non-active **11** (the complexes were scarcely soluble in other solvents). This study was performed for the HCT-116 cell line. Cell viability were very similar in both solvents (see Figures S19–S23) with the exception of compound **10** at high concentrations, showing better results for DMSO. Thus, the rest of the studies of this work were performed using DMSO, due to the higher solubility of the complexes.

The final concentration of DMSO/DMF in cell culture medium did not exceed 0.4%. Control cells were exposed to the maximum dose of solvent (DMF/DMSO 0,4% vol/vol) showing negligible toxicity (<6%) and used as 100% viability (Figure S24).

#### *Stability and speciation studies in DMSO- $d_6$ .*

The stabilities of compounds **7**, **8**, **9**, **10**, **13** and **14** were analysed by  $^1\text{H}$  NMR spectroscopy. These compounds were selected due to their cytotoxic activity or, in the case of **8** and **14**, because of the activity of their Pt(II) congeners. The complexes are not sufficiently soluble in  $\text{D}_2\text{O}$  and the studies were performed in  $\text{DMSO-}d_6$ , i.e., the solvent in which the stock solutions for biological studies were prepared (see Figures S25–S33). Because some cytotoxicity experiments were also performed in DMF, the stability was also studied in this solvent (see Figures S34–S40). It must be taken into account that when preparing samples for the cytotoxicity studies, the complexes are in DMSO (or DMF) solution a maximum time of 15 minutes before adding the culture medium. In any case, longer times were registered for this stability studies.

The stability of the Pt(II) derivatives **7**, **9** and **13** will be discussed first. In the case of **7**, when the  $\text{DMSO-}d_6$  solution was prepared, small resonances for the free ligand **L4** were observed and, after 5 hours, only the ligand signals were present in the spectrum (see Figure S25). In the case

of the DMF- $d_6$  solution the liberation of ligand is also observed, although partially (see Figure S34). Thus, this complex liberates the ligand rather easily. It must be considered that the benzoxazole unit is a weaker donor than the imidazole or aniline fragments present in complexes **9** and **13**, respectively, considering the  $pK_a$  values of these heterocycles as reference points ( $pK_a = 0.19$  for benzoxazole and around 5 for imidazole or aniline). Furthermore, it has been demonstrated in 'PdCl<sub>2</sub>' complexes that ligand **L4** is partially displaced by DMSO but not ligand **L1** [101].

The behaviour of **9** and **13** (DMSO- $d_6$ ) was clearly different. In the case of **9** (Figure S26), for the freshly prepared sample, the solution shows only the resonances of **9**. During the first hour, there was a significant decrement in the amount of **9**, while a new product, **9<sub>a</sub>'**, is quickly formed (see Figure S27) and a minor species, **9<sub>a</sub>''**, is also observed. After 1 hour, the **9:9<sub>a</sub>':9<sub>a</sub>''** ratio is 42:42:16. After this time, the amount of both **9** and **9<sub>a</sub>'** decreased slowly while **9<sub>a</sub>''** and a new species **9<sub>a</sub>'''** were gradually formed. After 16h, the major component of the mixture was **9<sub>a</sub>'''** (42%, see Table 5). We propose that **9<sub>a</sub>'** and **9<sub>a</sub>''** are the two mono-solvated species ([PtCl(DMSO)(**L5**)]<sup>+</sup>, **L5** is asymmetric), being **9<sub>a</sub>'** and **9<sub>a</sub>''** the products of kinetic and thermodynamic control, respectively. **9<sub>a</sub>'''** is proposed to be the di-solvated derivative [Pt(DMSO)<sub>2</sub>(**L5**)]<sup>2+</sup>. The uv-vis spectrum of **9** in DMSO was also registered (Figure S41). Two processes were detected (Figure S42), suggesting that the reactions leading to the mono-solvated complexes are not distinguished.

In the case of the <sup>1</sup>H NMR study of **13**, the formation of new species with time was observed (see Figures S28 and S29). The shape of the resonances in the region 8–8.2 ppm (where doublets are expected) reflects the overlapping of resonances of two species, that we propose are the two mono-solvated products [PtCl(DMSO)(**L7**)]<sup>+</sup>, **13<sub>a</sub>'**+**13<sub>a</sub>''**. At long reaction times, a small amount of free ligand **L7** is detected. See Table 5 for the ratio at 16 h. After 48h, the ratio is quite similar. The uv-vis spectrum of **13** in DMSO (see Figure S43) shows the presence of several isosbestic points and the analysis of the change in intensity at specific wavelengths (Figures S44-S46) reflects the presence of a sole process, which must correspond to the formation of the mono-aqua products.

**Table 5**

Ratio of the species formed after 16 hours when **9** or **13** are solved in DMSO-*d*<sub>6</sub> or DMSO-*d*<sub>6</sub>/D<sub>2</sub>O, 80:20<sup>a</sup>

Species formed	<b>9</b> <sup>b</sup>	<b>9</b> <sup>c</sup>	<b>13</b> <sup>b</sup>	<b>13</b> <sup>c</sup>
<b>X</b>	20	20	20	4
<b>X'</b>	15	5	68 <sup>d</sup>	86
<b>X''</b>	23	62		16
<b>X'''</b>	42	12	--	--
<b>Free ligand</b>	--	--	11 (L7)	--

<sup>a</sup> X represent the dichloride starting product, X' and X'' the two mono-solvated species and X''' the di-solvated complexes. In DMSO-*d*<sub>6</sub>, DMSO substitutes the chloride ligands and in DMSO-*d*<sub>6</sub>/D<sub>2</sub>O, 80:20, water enters into the coordination sphere. <sup>b</sup> DMSO-*d*<sub>6</sub>; <sup>c</sup> DMSO-*d*<sub>6</sub>/D<sub>2</sub>O, 80:20; <sup>d</sup> (X' + X'')

For Pt(IV) compounds **10** and **14** neither solvolysis products nor free ligand were observed after 16 hours and 2 days, respectively (DMSO-*d*<sub>6</sub>, Figures S30 and S31). Different behaviour was observed for **8** because the formation of a new Pt(IV) product, **8'**, (proposed to be a solvolysis species) and also free ligand **L4** were observed with time. After three days the ratio was **8/8'/L4** = 40/37/23 (Figure S32). The process was not inhibited by the addition of 10 equivalents of NaCl. This fact, along with the chemical shifts of the benzoxazole resonances of **8'** (resonance assignment made with the help of <sup>1</sup>H,<sup>1</sup>H-COSY, Figure S33) shifted to high field, led us to propose a substitution of the benzoxazole fragment by DMSO in **8'** ( $\kappa^1$ -**L4**), thus reflecting the hemilabile behaviour of **L4**. It is interesting to note that although Pt(IV) compounds are considered to be inert, their hydrolysis behaviour is currently under review – mainly due to their potential impact as prodrugs – and hydrolysis processes involving not only axial [102,103] but also equatorial [104] ligands have been reported.

#### 1.1. Aquation and speciation studies. Experimental and DFT analysis

It is known that DNA is the target of cisplatin [105,106] and that it undergoes aquation to form [Pt(NH<sub>3</sub>)<sub>2</sub>Cl(OH<sub>2</sub>)]<sup>+</sup> and [Pt(NH<sub>3</sub>)<sub>2</sub>(OH<sub>2</sub>)<sub>2</sub>]<sup>2+</sup> once inside the cell, a process that is facilitated by the low cellular concentration of chloride ions. The reported first-order rate constants for the first and second aquation steps in pure water are  $1.80 \times 10^{-4}$  and  $10.4 \times 10^{-5}$ , respectively [107], although other values, albeit similar, have been reported for different conditions [108,109]. The aquated forms of the complex are more reactive to the cellular targets. Although many cellular

components interact with cisplatin, DNA is the primary biological target of the drug. The platinum atom of the water adducts bind covalently to the N7 position of purines to afford primarily 1,2- or 1,3-intrastrand crosslinks and a lower number of interstrand crosslinks.[110] Considering that the second aquation takes place with a higher activation barrier, it has been suggested in numerous studies that cisplatin should bind to DNA in the mono-aquated form.[111,112] However, there has been some discussion concerning this issue and it has also been proposed that the di-aquated cisplatin [113] or both forms [114] react with DNA. Cisplatin–DNA adducts cause several cellular responses, such as replication arrest, transcription inhibition, cell-cycle arrest, DNA repair and apoptosis.[110,115] The reduced toxicity of carboplatin in comparison with cisplatin is usually explained by the fact that aquation of the malonate ligand is about one order slower.[116,117]

Thus, considering that aquation is a key step for in vivo activation of Pt drugs for metal-DNA interaction, we decided to study the aquation process of complexes **9** and **13** by uv-vis spectroscopy (H<sub>2</sub>O:DMSO = 95:5) and evaluate the complex speciation by <sup>1</sup>H NMR in DMSO-*d*<sub>6</sub>/D<sub>2</sub>O (80:20) mixtures. The complexes were not soluble in neat water. We have also performed a DFT study of the aquation process in the case of the most active complex **13**.

The <sup>1</sup>H NMR spectrum of **9** freshly solved in a DMSO-*d*<sub>6</sub>/D<sub>2</sub>O (80:20) mixture showed the presence of three species in a 1:6:2 ratio (see Figure S47 for a COSY spectrum and Figure S48 for the evolution with time). A comparison with those of the freshly solution of **9** in pure DMSO-*d*<sub>6</sub> suggests that the major component is the dichloride species, **9**. The minor component, called **9<sub>w</sub>'**, increased during the first hour and afterwards, it decreased until near disappearance after 16 hours (see Table 5 and Figure S49). On the contrary, the other component, called **9<sub>w</sub>''**, increases its relative intensity and becomes the major component after 16 hours. At long reaction times it is possible to observe a new minor species, **9<sub>w</sub>'''**.

If we compare the two solvolysis processes studied for **9** in DMSO-*d*<sub>6</sub> and DMSO-*d*<sub>6</sub>/D<sub>2</sub>O, some clear differences can be found: i) The process takes place faster in DMSO-*d*<sub>6</sub>:D<sub>2</sub>O than in DMSO-*d*<sub>6</sub> (compare Figures S27 and S49); ii) the ratio of solvate products at a given time is distinct in both solutions (Table 5); iii) the position of some resonances in both studies is clearly different (Figures S26 and S48). Taking together these results, we conclude the existence of an

important effect of the presence of water and that the solvolysis products in DMSO-*d*<sub>6</sub>:D<sub>2</sub>O involve the coordination of water molecules. To further demonstrate the substitution of the chloride ligands by water, the p*K*<sub>a</sub> of a DMSO/H<sub>2</sub>O (80:20) solution where the major component was **9<sub>w</sub>'** was determined. The initial pH value of the DMSO/H<sub>2</sub>O mixture was 8.1 and the p*K*<sub>a</sub> obtained was 6.52±0.20 (see Figure S54). This value is of the same order to that determined in other Pt(II) complexes with two N donor atoms [118–122]. Thus, **9<sub>w</sub>'** should be in the form of the deprotonated species ([PtCl(OH)(**L5**)]. It is proposed that both **9<sub>w</sub>'** and **9<sub>w</sub>'** have the same stoichiometry but are the products of kinetic and thermodynamic control, respectively. The species **9<sub>w</sub>'** should come from the displacement of two chloride ligands.

The uv-vis absorbance spectra between 250 and 800 nm of a 10<sup>-5</sup> M H<sub>2</sub>O:DMSO solution (95:5 ratio) of **9** was registered over time (Figure S50). The absorbance at a chosen wavelength was then plotted over time and the data were adjusted to a non-linear regression with the formula of a biexponential curve (inset of Figure 50):

$$y = ae^{bx} + ce^{dx} + e$$

where *y* = absorbance, *x* = time and *b* and *d* are rate constants of the first and second aquation steps, respectively.

The two processes observed are ascribed to the mono and di-aquation steps and the corresponding rate constants are reflected in Table 6.

When registering the evolution of **13** by <sup>1</sup>H NMR in a DMSO-*d*<sub>6</sub>/D<sub>2</sub>O (80:20) mixture, only one product was observed in the freshly prepared solution. The chemical shifts of the resonances are very similar to those of the species observed in the initial DMSO-*d*<sub>6</sub> solution (see Figure S51) and are assigned to the dichloride complex, **13**. After 5 minutes, a new species is detected, **13<sub>w</sub>'**. After 16 and 48 hours, this is the major component of the mixture. A minor component is also observed, **13<sub>w</sub>'** (see Figure S52). The ratio of the different species at 16 hours is reflected in Table 5. It is noteworthy the different evolution of **13** when comparing DMSO-*d*<sub>6</sub> or DMSO-*d*<sub>6</sub>/D<sub>2</sub>O (80:20) solutions (compare Figures S29 and S53) with a higher rate of solvation in the DMSO-*d*<sub>6</sub>/D<sub>2</sub>O mixture. Thus, the products formed when D<sub>2</sub>O is present, **13<sub>w</sub>'** and **13<sub>w</sub>'**, are tentatively assigned to the two mono-aquated complexes. We have determined a p*K*<sub>a</sub> value of 8.20±0.13

(Figure S55) for a DMSO/H<sub>2</sub>O (80:20) solution of **13** where the major component is **13w**<sup>?</sup>. Considering that the pH of the solvent mixture is 8.1, the two species: [PtCl(L7)(H<sub>2</sub>O)]<sup>+</sup> and [PtCl(OH)(L7)], should be in equilibrium and with a similar concentration.

In the uv-vis spectrum of **13** on H<sub>2</sub>O/DMSO (95:5, see Figure 7), two processes were observed. Considering that the two reactions of formation of the two mono-aquated species are not usually distinguishable by this technique, we propose that the reactions observed correspond to the formation of the mono- and di-aquated species. The fact that the di-aquated species is not detected by <sup>1</sup>H NMR may be due to the lower amount of D<sub>2</sub>O present in the NMR solution (the H<sub>2</sub>O/DMSO ratio of 95:5 does not allow to get the concentration to register a <sup>1</sup>H NMR spectrum). The values of the rate constants for the first and second aquation steps are shown in Table 6. The first aquation step is faster than the second. It is interesting to note that the values for **13**, i.e., the most cytotoxic derivative, are lower than those found for cisplatin, a fact that could lead to reduced side effects on using this complex as a metallodrug.

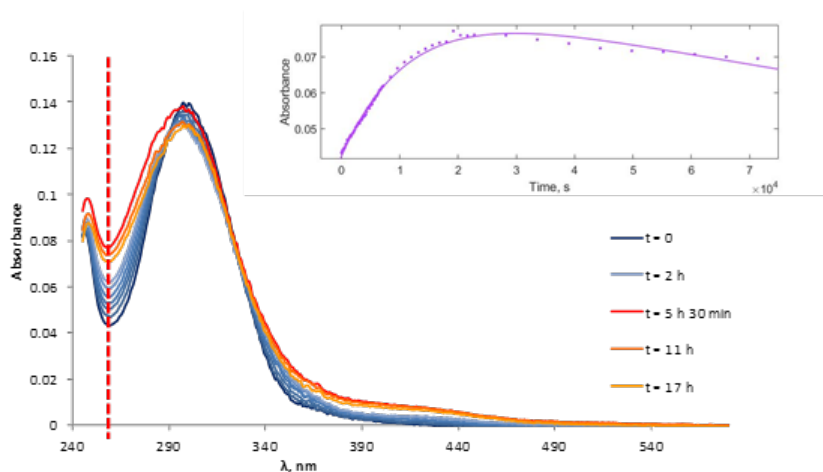


**Figure 7:** Absorbance spectra of compound **13** in DMSO:H<sub>2</sub>O (5:95) over time. Inset: Absorbance vs time at 259 nm.

**Table 6.**

Rate constants for the first ( $k_1$ ) and second ( $k_2$ ) aquation steps of compounds **9** and **13**, determined from the uv-vis measurements.

Complex	$k_1$	$k_2$
<b>9</b>	$1.011 (\pm 0.093) \cdot 10^{-3}$	$2.425 (\pm 0.41) \cdot 10^{-6}$
<b>13</b>	$8.346 (\pm 0.758) \cdot 10^{-5}$	$4.216 (\pm 0.743) \cdot 10^{-6}$

In the DFT studies of the aquation process of **13**, and considering the asymmetry of the N<sup>N</sup>' ligand, two reaction pathways were analysed [123,124]. In path A the first aquation takes place at the chloride trans to the aniline ring, while in path B it is the chloride trans to the benzimidazole heterocycle that is substituted by water in the first step. In both cases, the second step is the aquation of the second chlorine atom. The structures of the reactants, intermediates, transition states and products were optimised in water solvent ( $\epsilon = 78.35$ ) using the cluster-continuum model (SMD) [73].

It is widely accepted that ligand substitution in square-planar Pt(II) complexes is a concerted S<sub>N</sub>2 process [125] and previous DFT studies showed that in aqueous solution these reactions proceed through a single pentacoordinate transition state [126,127]. We were able to find the pentacoordinate TS for both paths with their imaginary frequencies (Table S8). Selected distances and angles for stationary points along the reaction pathway on the potential energy surface (the reactant, TS and products) are gathered in Table S9 and the corresponding structures are shown in Figures S56 and S57. In all cases, and as previously observed in other studies [124,128], the replacement of Cl<sup>-</sup> by H<sub>2</sub>O on the Pt centre occurs through a distorted trigonal bipyramidal transition state (TS) in which the central metal atom, the Cl<sup>-</sup> leaving group and the incoming H<sub>2</sub>O molecule are in the equatorial plane with a small Cl–Pt–O angle (66.3–69.3°). In all cases, the Pt–Cl bond distance increases as the water molecule approaches the metal centre, until the transition geometry is reached. In the transition states, the distances of the bonds that are being broken (Pt–Cl) or formed (Pt–O) are about 15–20% longer than the distances found in the reactant or products, with similar percentages for the bonds of the ligands that are entering or leaving the coordination sphere reflecting a synchronous concerted mechanism.

The free energy profiles of the first and second aquation steps are provided in Figure 8 and the free Gibbs energies ( $\Delta G^\ddagger$ ) and rate constants ( $k$ ) are gathered in Table 7. The free energy of activation for the first step is similar for both paths and while this value for the second step is higher in path B, we consider that the difference is not significant enough to determine that path A is the only one for aquation. Besides, the experimental rate constant values lie between the

values obtained for the two both paths. Thus, we propose that both alternatives for aquation may be in operation, although path A may be preferred for a major fraction of the molecules. Taking into account the small difference between the corresponding activation energies for the first and second steps through path A, we propose that the complex can interact with DNA in both the mono- and diaquated form, as previously concluded in other studies [113]. The values for the free energy of activation for **13** are relatively similar to those of cisplatin [112] and somewhat lower than those found for carboplatin [117] and oxaliplatin [117], with these two complexes exhibiting a higher barrier for the first than the second step. The aquation reactions for **13** are endothermic, with free energy values of 4.6–4.7 Kcal.mol<sup>-1</sup> except for the second step of path B (7.2 Kcal.mol<sup>-1</sup>).

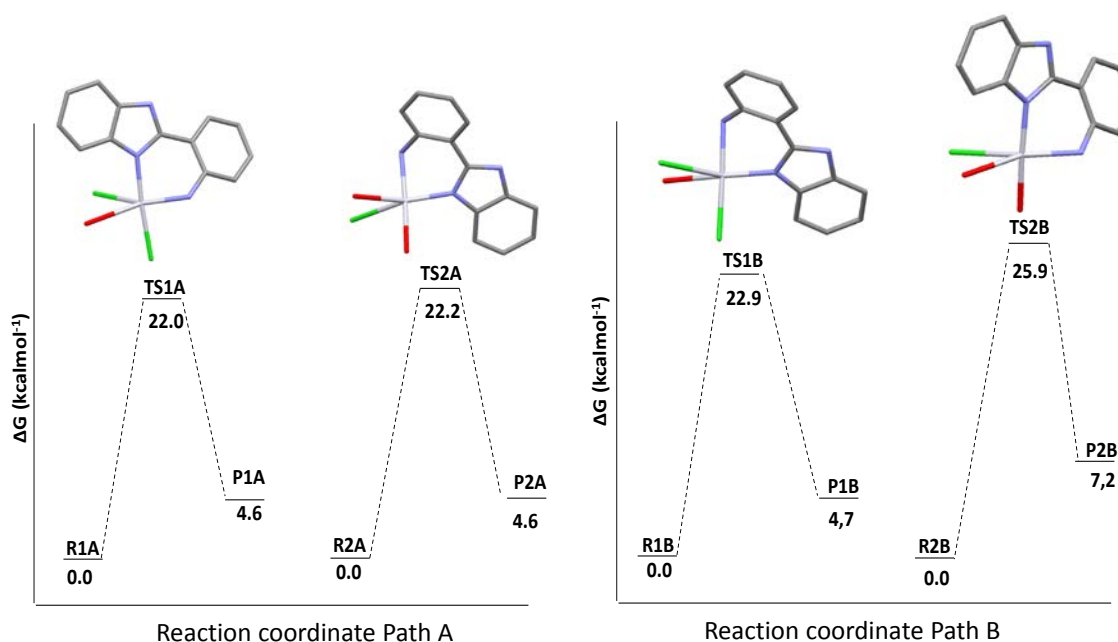


**Figure 8.** Free energy profiles of the first and second aquation steps for complex **13** along paths A and B in the SMD/H<sub>2</sub>O model at the B3LYP-D3/6-311++G(d,p) /LAN2DZ +f level of theory.

**Table 7**

Gibbs free energies ( $\Delta G^\ddagger$ ) and rate constants (k) for aquation reactions of complex **13** (parameters calculated at the B3LYP-D3 level of theory).

	$\Delta G^\ddagger_{1A}$ (kcal/mol)	$k_{1A}$ (l/mol.s)	$\Delta G^\ddagger_{2A}$ (kcal/mol)	$k_{2A}$ (l/mol.s)
<b>Path A</b>	22.00	$2.1 \times 10^{-4}$	22.20	$1.49 \times 10^{-4}$
	$\Delta G^\ddagger_{1B}$ (kcal/mol)	$k_{1B}$ (l/mol.s)	$\Delta G^\ddagger_{2B}$ (kcal/mol)	$k_{2B}$ (l/mol.s)
<b>Path B</b>				

22.90	4.45 x 10 <sup>-5</sup>	25.88	2.61 x 10 <sup>-7</sup>
-------	-------------------------	-------	-------------------------

Structural details of the reactants, transition states and products for both paths can be found in the Supporting Information as separate files along with the structures of all species.

### 1.2. DNA binding.

Agarose gel electrophoresis was used to study the ability of the compounds to bind to DNA. Compounds **7**, **9**, **10** and **13** were analysed using the supercoiled DNA plasmid pUC18. Initially, the plasmid is mostly in a supercoiled form (Form I), although DNA manipulation can introduce breaks, for example by mechanical shear, which can generate some uncoiling of the plasmid that can be then detected in control samples (open circular form or form II) [129]. When a compound interacts with the plasmid, it changes to the open circular form, which migrates slower than the supercoiled form. If the compound is able to cleave double strands, a linear form (Form III) is generated that will migrate between form 1 and form 2. The difference in mobility of these three forms allows us to ascertain whether a given compound binds with DNA.

Compounds **7**, **9** and **13** interact with DNA reflecting that, as expected, [130] DNA is possibly the target of the compounds under investigation. The interaction is observed on using concentrations from 100  $\mu$ M in the case of **9** and from 150  $\mu$ M in the case of **7**, which are able to transform the plasmid to its open circular form (Figure 9). Compound **13** shows higher affinity to DNA than **7** or **9** as it interacts with the plasmid at a lower concentration (25  $\mu$ M) and cleaves the pUC18 plasmid at higher concentrations (100  $\mu$ M). This relatively high affinity of **13** for DNA may explain the better IC<sub>50</sub> values obtained with this compound. It is to note the effect of the presence of DMSO in the behaviour of cisplatin, according to previous reported studies [99]. A similar effect was observed in the presence of DMF (see figure S58).

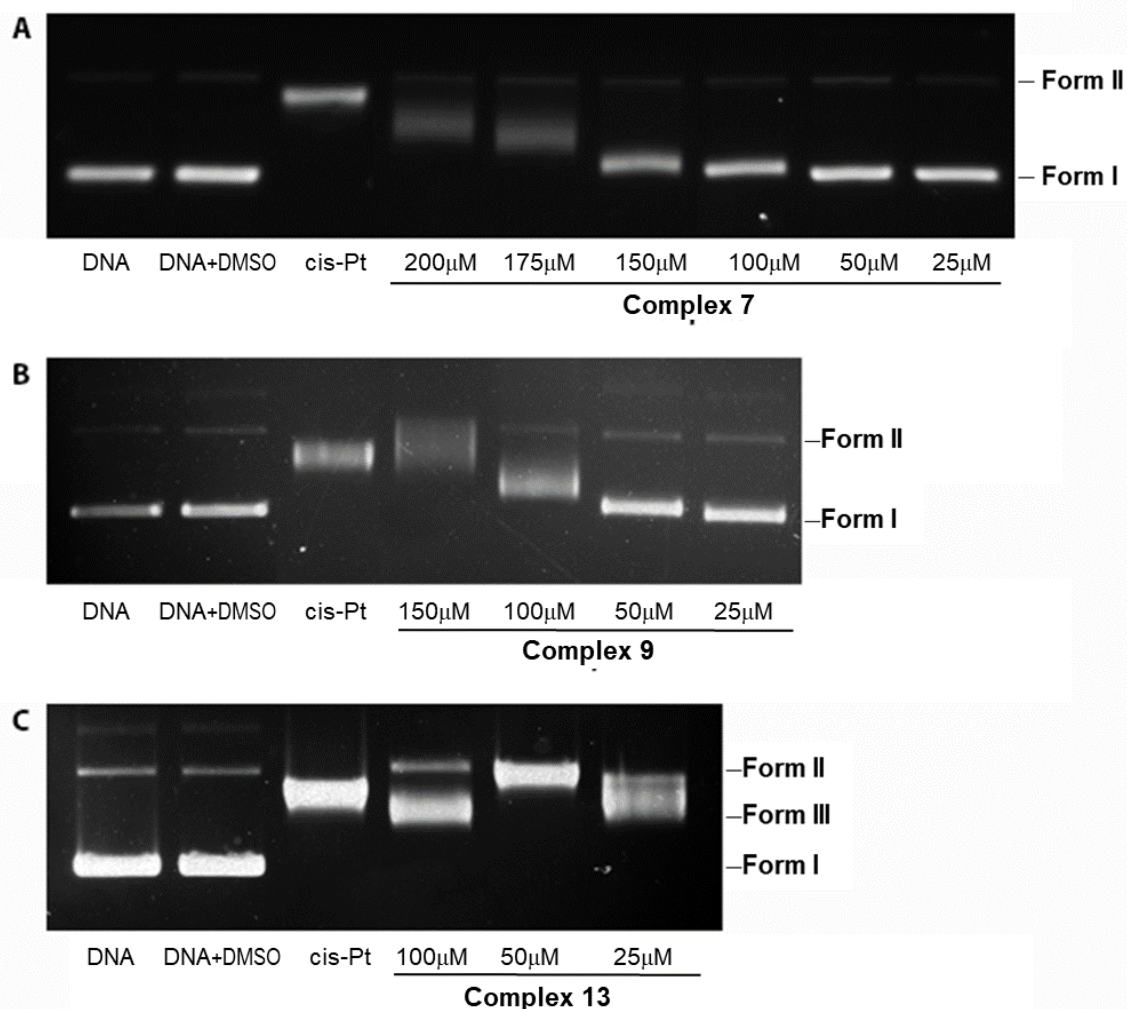


**Figure 9:** Agarose gel electrophoresis of compounds **7** (A), **9** (B), and **13** (C). See Experimental Section for conditions

As expected, the analogous Pt(IV) compounds (**8**, **10** and **14**) did not interact with DNA, even at the highest concentrations. Additional studies were performed to compare the interaction of the Pt(II) compounds and their Pt(IV) analogues in the absence and presence of sodium ascorbate (Figure 10 for complex **10** and Figures S59 and S60 for complexes **8** and **14**, respectively). In the presence of ascorbate, the Pt(IV) compounds **8** and **10** showed DNA interaction in a similar way to their Pt(II) congeners, **7** and **9**, respectively, reflecting that a reduction process has taken place. In the case of **14** the interaction with DNA seems to be very weak. See below for more studies concerning the behaviour of these Pt(IV) complexes.

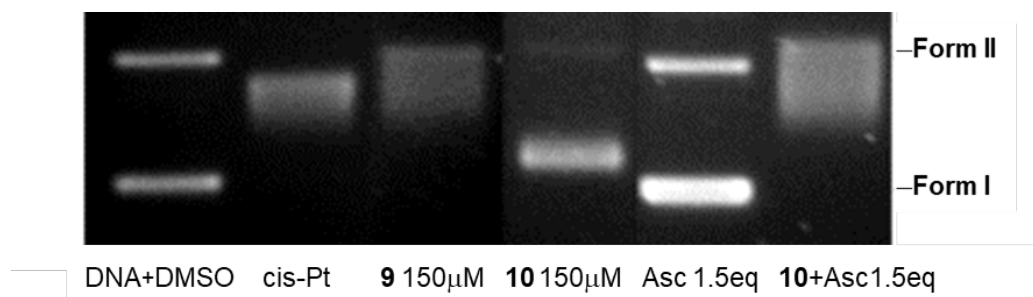


**Figure 10:** Agarose gel electrophoresis of compounds **9**, **10**, and **10** in the presence of 1.5 equivalents of ascorbate (the concentration of **10** when adding ascorbate is 150  $\mu$ M).

### 1.3. Cell death mechanism.

Apoptosis induced by compounds **7** and **13** was evaluated by flow cytometry using IP/Annexin V staining in the A549 cell line. As shown in Figures 11 and 12, compound **7** did not modulate the basal level of apoptosis. However, compound **13** induced a potent apoptotic response in A549 cells in a dose-dependent fashion. In addition, the apoptotic effect of **13** was also evaluated in other cancer-derived cell lines as HCT116, HT29 and MCF7, with a marked apoptotic response observed in all cases (Figure S61). Therefore, all the evidence indicate that, as expected for a Pt(II) complex, [130] cell death associated with **13** correlates with an apoptotic response in our experimental model. Furthermore, the data obtained in a cell line as HT29, with mutated p53[131] suggest that the induction of apoptosis could be in a p53-independent fashion. This observation is especially interesting considering that the tumor suppressor p53 is one of the key determinants of the cellular response to current chemotherapy cisplatin [132].

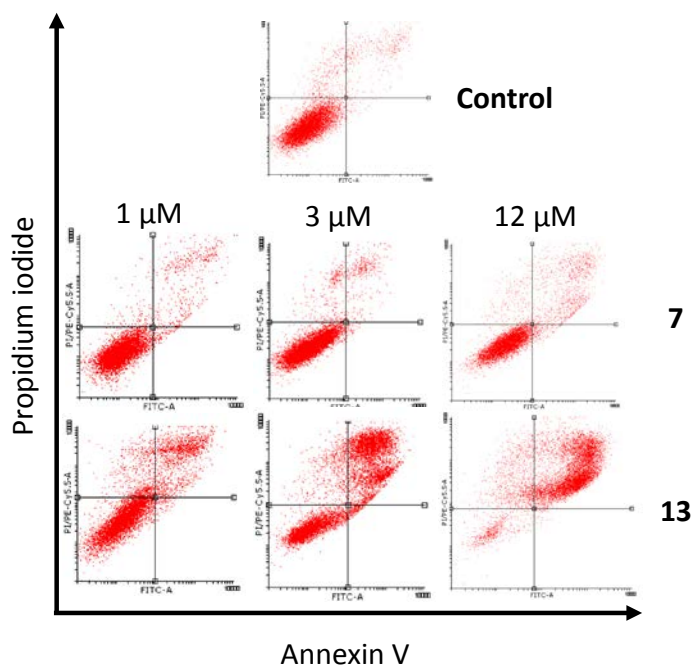


**Figure 11.** A549 cells were treated with the indicated concentrations of compounds **7** and **13** for 24 hours and then stained with Annexin V-FITC/Propidium Iodide for assay by flow cytometry. Control signifies treated cells with the same amount of vehicle (DMSO). The image shows a representative single experiment (dot plot) out of three. As shown, compound **7** was unable to promote apoptosis after 24 hours of incubation at different concentrations while compound **13** promoted a marked increase in apoptosis under the same conditions.

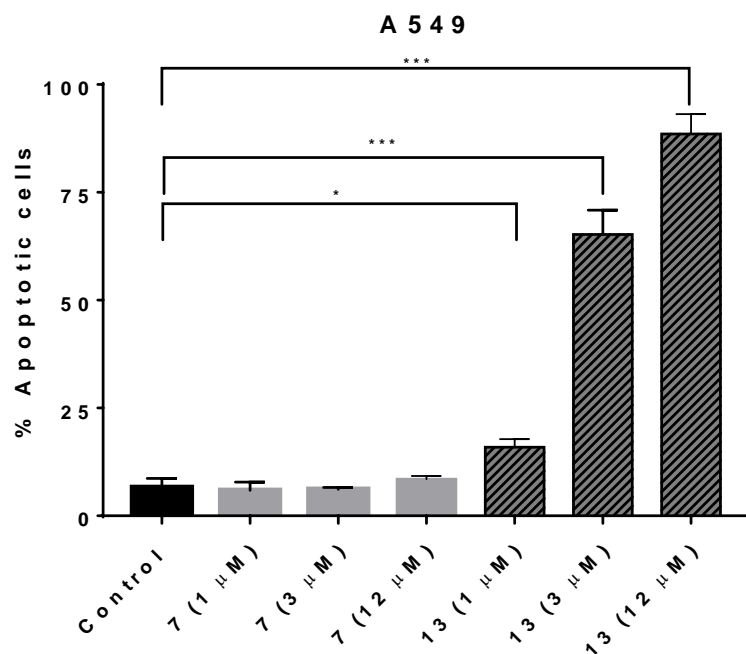


**Figure 12.** Histogram showing the average of three independent experiments to evaluate the percentage of apoptotic cells after incubating A549 cells with compounds **7** or **13** as in Figure 11. Data are presented as mean  $\pm$  standard deviation. The statistical significance of differences was evaluated by Student's t-test using GraphPad Prism software. \* $p < 0.05$ , \*\* $p < 0.01$  and \*\*\* $p < 0.001$ .

#### 1.4. Haemolytic activity.

It has been reported that repeated intravenous administration of platinum salts may induce haemolytic anaemia by interfering with iron metabolism, decreasing the level of red blood cell precursors and creating an immune-complex between red blood cells (RBC) and cisplatin [133].

Thus, with the aim of gaining some insight into the general toxicity of the complexes, the most cytotoxic derivatives **7**, **9**, **10** and **13** were selected for haemolytic studies [134] using erythrocytes from fresh swine blood. Triton X-100 surfactant was used to achieve complete haemolysis as a positive control. The four complexes were non-haemolytic at concentrations up to 50  $\mu\text{M}$  (Table 8), which is between 3- and 40-fold higher than the  $\text{IC}_{50}$  values determined in vitro. It is noteworthy that high levels of haemolytic activity were reported for cisplatin (75% at 100  $\mu\text{M}$ ) [135].

**Table 8**

Percentage of haemolysis H(%) induced by compounds **7**, **9**, **10** and **13** at different concentrations.

	5 $\mu\text{M}$	10 $\mu\text{M}$	25 $\mu\text{M}$	50 $\mu\text{M}$
<b>7</b>	< 1	< 1	< 1	1.2
<b>9</b>	< 1	< 1	< 1	< 1
<b>10</b>	< 1	< 1	< 1	< 1
<b>13</b>	< 1	< 1	< 1	< 1

In all cases the compounds did not interact with erythrocytes, even at high concentrations.

#### 1.5. Behaviour of the Pt(IV) complexes **8**, **10** and **14**. Cellular uptake and measure of standard reduction potentials.

As stated, the Pt(IV) complexes, **8**, **10** and **14**, whose Pt(II) congeners were cytotoxic, exhibited different behaviour in this respect. Only complex **10** was cytotoxic in the HCT116 cell line but **8** and **14** showed  $\text{IC}_{50}$  values above 25  $\mu\text{M}$  in all cell lines studied. This lack of activity

of the latter two compounds can be explained by two main reasons: an inability to enter the cells or incomplete reduction.

In an effort to obtain more information, the cellular uptake of compounds **7**, **8**, **13** and **14** was studied by ICP-mass spectroscopy (the congeners of Pt(II), **7** and **13**, were also studied for the sake of comparison). To this end, MCF7 cells were exposed to the compounds at a concentration equivalent to the IC<sub>50</sub> of the corresponding cytotoxic Pt(II) analogue (5 μM for **7** and **8** and 5 μM for **13** and **14**, respectively) for three hours. Cisplatin was included at the same concentrations as a reference. The results (see Table 9) show that all of the compounds were able to enter inside cells, with higher accumulation rates obtained than for cisplatin. Higher values were obtained for the Pt(II) derivatives than for the Pt(IV) analogues. Compound **13** entered the cells at more than twice the level as compound **14**, whereas compound **7** has an accumulation rate three times higher than its Pt(II) analogue. These results rule out the inability to enter into the cells as the reason for the lack of cytotoxicity.

**Table 9**  
Pt concentration inside MCF7 cells.

Comp.	Pt concentration (ppb)
<b>7</b> (5 μM)	41.53 ± 5.89
<b>8</b> (5 μM)	13.41 ± 1.73
<b>13</b> (2 μM)	38.78 ± 2.93
<b>14</b> (2 μM)	16.84 ± 2.27
<b>Cisplatin</b> (2 μM)	1.5 ± 0.24
<b>Cisplatin</b> (5 μM)	3.07 ± 0.62

The possible reduction of **8**, **10** and **14** with ascorbic acid (10 equiv) was also examined by <sup>1</sup>H NMR spectroscopy on DMSO-*d*<sub>6</sub> solutions. In the case of **10**, evidence for the reduction to the corresponding Pt(II) congener, **9**, was observed and the product of the first aquation of **9** (**9<sub>a</sub>'**) was also seen. After three days the ratio was as follows: **10**/**9**/**9<sub>a</sub>'** = 50/41/9 (Figure S62). This

behaviour is typical of a Pt(IV) prodrug with the necessary prior reduction to Pt(II) to undergo the solvolysis processes that leads to the active species in the binding to DNA.

Reduction was not observed after the addition of ascorbic acid to a solution of **14** even after two days (Figure S63). Thus, this complex is inert towards solvolysis and reduction under the conditions applied.

When complex **8** was reacted with ascorbic acid, besides the solvolysis product already observed in the absence of the reducing agent, the presence of a high amount of free ligand **L4** was also detected (Figure S64). The ratio after 24 hours and three days was  $\mathbf{8'}/\mathbf{L4} = 30/70$ . Complex **7** was not detected but the large amount of **L4**, which was much higher than that observed after three days with **8** in DMSO solution (23%), and the instability of **7** (see above) led us to propose that reduction of **8** to **7** and fast liberation of the free ligand from **7** takes place.

These NMR observations fit with the behaviour observed for **8**, **10** and **14** in the electrophoretic experiments. As stated previously, in the presence of ascorbate, complexes **8** and **10** showed DNA interaction, as their Pt(II) congeners, but the interaction was very weak in the case of **14**.

As far as the reduction process is concerned, if we consider the peak potentials (Table 2) then the ease of reduction of the Pt(IV) compounds follows the order:  $\mathbf{14} < \mathbf{10} < \mathbf{8}$ . This is not in accordance with complex **10** being the only one to exhibit cytotoxicity. However, as stated in the introduction, there is some controversy around the predictive ability of the peak potentials ( $E_p$ ) obtained from cyclic voltammetry studies on the reduction of Pt(IV) compounds and the determination of standard reduction potentials ( $E^\ominus$ ) has been proposed as a more reliable approach [55]. Thus, we decided to determine  $E^\ominus$  for complexes **8**, **10** and **14** by registering the cyclic voltammograms at different scan rates (see Supporting Information, Figures S65–S73 and experimental part for the methodology). When  $I_p$  is plotted against scan rate (Figures S74A-S76 A) or against the square root of scan rate (Figures S74B-S76B) for the three complexes,  $I_p$  increases with scan rate and shows a linear relationship with the square root of scan rate. This suggests that the reduction on the surface of the Pt electrode is a typical diffusion controlled electrochemical process. The  $E^\ominus$  values are provided in Table 10 and reflect the following order

of increasing reduction potentials  $14 < 8 < 10$ . The reduction of **10** and **8**, observed by NMR (with ascorbic acid) and its binding to DNA (similar to its Pt(II) congeners, see above), as deduced by agarose gel electrophoresis in the presence of ascorbate (Figures 10, S62 and S64), are consistent with this order of reduction potentials (the reduction potential of ascorbic acid at pH = 7 is 0.27 V) [136]. In accordance with these data, reduction was not observed by NMR for **14** and only a small change in the DNA band was detected, which could be due to a weak interaction, in clear contrast with the strong binding observed with its Pt(II) congener **13**. In any case – and considering the notable difference in  $E^\ominus$  values between **8** and **10** – we propose that the lack of cytotoxicity of complexes **8** and **14** may be due to a difficulty in the reduction process under biological conditions.

**Table 10**

Standard reduction potentials ( $E^\ominus$ ) for complexes **10**, **8** and **14** vs Ag/AgCl.

Complex	<b>10</b>	<b>8</b>	<b>14</b>
$E^\ominus$ (v)	0.26±0.17	-0.29±0.13	-0.47±0.01

## 2. Conclusions

In order to perform an SAR study with Pt(II) compounds and to verify the potential of Pt(IV) derivatives, a set of fourteen dichloride Pt(II) and tetrachloride Pt(IV) compounds containing different arylazole heterocyclic ligands acting as bidentate chelates has been synthesised and fully characterised. Stacking interactions (Pt···Pt and/or  $\pi$ - $\pi$ ) in the square-planar Pt(II) or octahedral Pt(IV) complexes, whose structure was determined by X-ray diffraction, were detected.

The ‘Pt(II)Cl<sub>2</sub>’ derivatives containing 2-(2'-pyridyl)benzoxazole (complex **7**), 2-(2'-pyridyl)imidazole (**9**) and especially that containing 2-(1H-benzimidazol-2-yl)aniline (**13**) were found to be cytotoxic to different degrees against A549, MCF7, HCT116 and HT29 cancer cell lines, with the limit of study being a 25  $\mu$ M concentration. Complex **13** was notably more active than cisplatin. Similarly to cisplatin, two aquation or solvolysis (DMSO) processes were observed for **9** and **13** while **7** lost the ligand easily. For the most active complex **13**, an in-depth analysis by DFT calculations of the two aquation processes was carried out. It was found that the two pathways for the first aquation, considering the asymmetry of the N<sup>^</sup>N' ligand, were possible and

that the second aquation was also feasible. It was verified that DNA was the target by means of agarose gel electrophoresis and that the cell death took place by apoptosis in the case of **13**. A positive finding for possible future use as drugs is that the cytotoxic derivatives did not exhibit haemolytic activity.

Although the three Pt(IV) congeners of the Pt(II) active complexes entered into the cells (MCF7), only one Pt(IV) compound, [PtCl<sub>4</sub>(**L5**)] (**10**), the congener of complex **9**, was cytotoxic in the HCT116 cell line. What concerns the reduction process, it was concluded that the peak reduction potential is not a useful parameter to predict the ability for reduction. However, a correlation between the cytotoxic activity and the standard reduction potential,  $E^\ominus$ , obtained by measuring cyclic voltammetry experiments at different scan rates, was found.

In conclusion, compounds with formula [PtCl<sub>4</sub>(N<sup>^</sup>N<sup>'</sup>)] are not the best candidates for Pt(IV) prodrugs. In any case, it has been demonstrated that not only the axial ligands but also the equatorial ones affect the reduction process and one important conclusion is that the standard reduction potential ( $E^\ominus$ ), and not the peak potential, may be a parameter of interest as a predictive tool for future studies concerning the use of Pt(IV) derivatives as anticancer prodrugs. Besides, we have demonstrated the positive effect on the cytotoxic activity of an aniline fragment in a N<sup>^</sup>N<sup>'</sup> ligand in [PtCl<sub>2</sub>(N<sup>^</sup>N<sup>'</sup>)] complexes, a fact that may pave the way to study other Pt complexes with heterocyclic bidentate ligands containing this ring.

**Appendix A. Supplementary data.** cif files. x,y,z files from DFT calculations. Synthesis and general characterization of complexes and NMR data. Crystal data, Figures and Tables of the intermolecular interactions. Cyclic voltammograms. Electronic spectra. DFT studies. Aquation processes. NMR studies of the stability in solution and reduction process of Pt(IV) compounds. Information from biological studies. The following files are available free of charge.

## **Funding**

This work has been funded by the Spanish Ministerio de Ciencia, Innovación y Universidades (MCIU), Agencia Estatal de Investigación (AEI) and Fondo Europeo de Desarrollo Regional (FEDER) (RTI2018-100709-B-C21 to BRM, RTI2018-100709-B-C22 to AM, RTI2018-094093-B-I00 to RSP), Junta de Comunidades de Castilla-La Mancha-FEDER (JCCM) (grant SBPLY/19/180501/000260 to BRM), Ministerio de Economía y Competitividad (Project PID2019-104381GB-I00 to GC), Fundación Leticia Castillejo Castillo to MJRH, Junta de Castilla y León, Consejería de Educación y Cultura y Fondo Social Europeo (Projects BU263P18 and BU087G19 to JVC) as well as UCLM-FEDER (grants 2019-GRIN-27183 and 2019-GRIN-27209 to BRM) and University of Girona (MPCUdG2016/076 to AM).

## References

- [1] B. Rosenburg, L. Van Camp, T. Krigas, Inhibition of Cell Division in *Escherichia coli* by Electrolysis Products from a Platinum Electrode, *Nature*. 205 (1965) 698–699.
- [2] K.M. Deo, D.L. Ang, B. McGhie, A. Rajamanickam, A. Dhiman, A. Khoury, J. Holland, A. Bjelosevic, B. Pages, C. Gordon, J.R. Aldrich-Wright, Platinum coordination compounds with potent anticancer activity, *Coord. Chem. Rev.* 375 (2018) 148–163. <https://doi.org/10.1016/j.ccr.2017.11.014>.
- [3] J. Reedijk, Platinum Anticancer Coordination Compounds : Study of DNA Binding Inspires New Drug Design, *Eur. J. Inorg. Chem.* 2009,. (2009) 1303–1312. <https://doi.org/10.1002/ejic.200900054>.
- [4] N. Cutillas, G.S. Yellol, C. De Haro, C. Vicente, V. Rodríguez, J. Ruiz, Anticancer cyclometalated complexes of platinum group metals and gold, *Coord. Chem. Rev.* 257 (2013) 2784–2797. <https://doi.org/10.1016/j.ccr.2013.03.024>.
- [5] C. Desoize, B; Madoulet, Particular aspects of platinum compounds used at present in cancer treatment, *Rev. Oncol. Hemat.* 42 (2002) 317–325. [https://doi.org/10.1016/s1040-8428\(01\)00219-0](https://doi.org/10.1016/s1040-8428(01)00219-0)
- [6] M. Galanski, M.A. Jakupec, B.K. Keppler, Update of the Preclinical Situation of Anticancer Platinum Complexes : Novel Design Strategies and Innovative Analytical

- Approaches, *Curr. Med. Chem.* 12 (2005) 2075–2094.  
<https://doi.org/10.2174/0929867054637626>
- [7] N.J. Wheate, S. Walker, G.E. Craig, R. Oun, The status of platinum anticancer drugs in the clinic and in clinical trials, *Dalton Trans.* 39 (2010) 8113–8127.  
<https://doi.org/10.1039/c0dt00292e>.
- [8] T.C. Johnstone, K. Suntharalingam, S.J. Lippard, Third row transition metals for the treatment of cancer, *Philos. Trans. A Math. Phys. Eng. Sci.* 373 (2015) 20140185.  
<https://doi.org/10.1098/rsta.2014.0185>
- [9] R. Oun, Y.E. Moussa, N.J. Wheate, The side effects of platinum-based chemotherapy drugs: a review for chemists, *Dalton Trans.* 47 (2018) 6645–6653.  
<https://doi.org/10.1039/C8DT00838H>.
- [10] T.C. Johnstone, J.J. Wilson, S.J. Lippard, Monofunctional and Higher-Valent Platinum Anticancer Agents, *Inorg. Chem.* 52 (2013) 12234–12249.  
<https://doi.org/10.1021/ic400538c>
- [11] U. Kalinowska-lis, J. Ochocki, K. Matlawska-wasowska, Trans geometry in platinum antitumor complexes, 252 (2008) 1328–1345. <https://doi.org/10.1016/j.ccr.2007.07.015>.
- [12] S. Dilruba, G. V Kalayda, Platinum-based drugs: past, present and future, *Cancer Chemother. Pharmacol.* 77 (2016) 1103–1124. <https://doi.org/10.1007/s00280-016-2976-z>.
- [13] T.C. Johnstone, K. Suntharalingam, S.J. Lippard, The Next Generation of Platinum Drugs: Targeted Pt(II) Agents, Nanoparticle Delivery, and Pt(IV) Prodrugs, *Chem. Rev.* 116 (2016) 3436–3486. <https://doi.org/10.1021/acs.chemrev.5b00597>.
- [14] L. Cai, C. Yu, L. Ba, Q. Liu, Y. Qian, B. Yang, C. Gao, Anticancer platinum - based complexes with non - classical structures, *Appl. Organomet. Chem.* 32 (2017) e4228.  
<https://doi.org/10.1002/aoc.4228>.
- [15] G. Facchetti, I. Rimoldi, *Bioorganic & Medicinal Chemistry Letters* Anticancer platinum (II) complexes bearing N -heterocycle rings, *Bioorg. Med. Chem. Lett.* 29 (2019) 1257–1263. <https://doi.org/10.1016/j.bmcl.2019.03.045>.

- [16] L. Bai, C. Gao, Q. Liu, C. Yu, Z. Zhang, L. Cai, B. Yang, Y. Qian, J. Yang, X. Liao, Research progress in modern structure of platinum complexes, *Eur. J. Med. Chem.* 140 (2017) 349–382. <https://doi.org/10.1016/j.ejmech.2017.09.034>.
- [17] I. Łakomska, M. Jakubowski, M. Barwiołek, T. Muzioł, Different bonding of triazolopyrimidine to platinum (IV). Structural and in vitro cytotoxicity studies, *Polyhedron*. 160 (2019) 123–129. <https://doi.org/10.1016/j.poly.2018.12.022>.
- [18] Y. Zhao, N.J. Farrer, H. Li, J.S. Butler, R.J. Mcquitty, A. Habtemariam, F. Wang, P.J. Sadler, De Novo Generation of Singlet Oxygen and Ammine Ligands by Photoactivation of a Platinum Anticancer Complex, *Angew. Chem. Int. Ed. Engl.* 52 (2013) 13633–13637. <https://doi.org/10.1002/anie.201307505>.
- [19] W.N.J. William, B.S. Glisson, Novel strategies for the treatment of small-cell lung carcinoma, *Nat. Rev. Clin. Oncol.* 8 (2011) 611–619. <https://doi.org/10.1038/nrclinonc.2011.90>
- [20] R.F. Murphy, N. Farrell, A. Aguila, M. Okada, F.M. Balis, T. Fojo, Accumulation of Novel Transplatinum Complexes in Cisplatin and Oxaliplatin Resistant Cell Lines Overcomes Resistance, *Proc. Am. Assoc. Cancer Res.* 46 (2005) 4109. <https://doi.org/10.2174/187152007779314080>
- [21] L.R. Kelland, J. Barnard, K. Mellish, P. Goddard, B. Murrer, K. Harrap, A Novel trans-Platinum Coordination Complex Possessing in Vitro and in Vivo Antitumor Activity, *Cancer Res.* 54 (1994) 5618–5622.
- [22] W.I. Sundquist, D.P. Bancroft, S.J. Lippard, Synthesis, Characterization, and Biological Activity of cis-Diammineplatinum (II) Complexes of the DNA Intercalators 9-Aminoacridine and Chloroquine, *J Am. Chem. Soc.* 112 (1990) 1590–1596.
- [23] K.S. Lovejoy, R.C. Todd, S. Zhang, M.S. McCormick, J.A.D. Aquino, J.T. Reardon, A. Sancar, K.M. Giacomini, S.J. Lippard, cis-Diammine(pyridine)chloroplatinum(II), monofunctional platinum(II) antitumor agent: Uptake, structure, function, and prospects, *Proc Natl Acad Sci USA.* 105 (2008) 8902–8907. <https://doi.org/10.1073/pnas.0803441105>

- [24] G.Y. Park, J.J. Wilson, Y. Song, S.J. Lippard, Phenanthriplatin, a monofunctional DNA-binding platinum anticancer drug candidate with unusual potency and cellular activity profile, *Proc Natl Acad Sci USA*. 109 (2012) 11987–11992.  
<https://doi.org/10.1073/pnas.1207670109>.
- [25] K. Huang, Z. Chen, Y. Liu, Z. Li, J. Wei, M. Wang, X.-L. Xie, H. Liang, Platinum(II) complexes containing aminophosphonate esters: Synthesis, characterization, cytotoxicity and action mechanism, *Eur. J. Med. Chem.* 64 (2013) 554–561.  
<https://doi.org/10.1016/j.ejmech.2013.04.024>.
- [26] X. Song, Y. Liu, J. Shao, Z. Zhang, C. Xie, X. Qiao, W. Bao, J. Xu, Rapid induction of apoptosis in tumor cells treated with a new platinum(II) complex based on amino-thiazolidinone, *Eur. J. Med. Chem.* 157 (2018) 188–197.  
<https://doi.org/10.1016/j.ejmech.2018.07.075>.
- [27] K.E. Prosser, S.W. Chang, F. Saraci, P.H. Le, C.J. Walsby, Anticancer copper pyridine benzimidazole complexes: ROS generation, biomolecule interactions, and cytotoxicity, *J. Inorg. Biochem.* 167 (2017) 89–99. <https://doi.org/10.1016/j.jinorgbio.2016.11.006>.
- [28] N. Ferri, S. Cazzaniga, L. Mazzarella, G. Curigliano, G. Lucchini, D. Zerla, R. Gandolfi, G. Facchetti, M. Pellizzoni, I. Rimoldi, Cytotoxic effect of (1-methyl-1 H-imidazol-2-yl)-methanamine and its derivatives in Pt II complexes on human carcinoma cell lines: A comparative study with cisplatin, *Bioorg. Med. Chem.* 21 (2013) 2379–2386.  
<https://doi.org/10.1016/j.bmc.2013.01.063>.
- [29] D. Gibson, Platinum(IV) anticancer prodrugs – hypotheses and facts, *Dalton Trans.* 45 (2016) 12983–12991. <https://doi.org/10.1039/c6dt01414c>.
- [30] R.G. Kenny, W. Chuah, A. Crawford, C.J. Marmion, Platinum (IV) Prodrugs – A Step Closer to Ehrlich’s Vision ?, *Eur. J. Inorg. Chem.* (2017) 1596–1612.  
<https://doi.org/10.1002/ejic.201601278>.
- [31] M.D. Hall, W. Hambley, Platinum (IV) antitumour compounds : their bioinorganic chemistry, *Coord. Chem. Rev.* 232 (2002) 49–67. [https://doi.org/10.1016/S0010-8545\(02\)00026-7](https://doi.org/10.1016/S0010-8545(02)00026-7)

- [32] M.D. Hall, H.R. Mellor, R. Callaghan, T.W. Hambley, Perspective Basis for Design and Development of Platinum(IV) Anticancer Complexes, *J. Med. Chem.* 50 (2007) 3403–3411. <https://doi.org/10.1021/jm070280u>.
- [33] Z. Wang, Z. Deng, G. Zhu, Emerging platinum(IV) prodrugs to combat cisplatin resistance: from isolated cancer cells to tumor microenvironment, *Dalton Trans.* 48 (2019) 2536–2544. <https://doi.org/10.1039/c8dt03923b>.
- [34] M. Crespo, Cyclometallated platinum(IV) compounds as promising antitumour agents, *J. Organomet. Chem.* 879 (2019) 15–26. <https://doi.org/10.1016/j.jorganchem.2018.10.008>.
- [35] M. Sinisi, F.P. Intini, G. Natile, Dependence of the Reduction Products of Platinum(IV) Prodrugs upon the Configuration of the Substrate, Bulk of the Carrier Ligands, and Nature of the Reducing Agent, *Inorg. Chem.* 51 (2012) 9694–9704. <https://doi.org/10.1021/ic300957v>.
- [36] T. Babu, A. Sarkar, S. Karmakar, C. Schmidt, D. Gibson, Multiaction Pt(IV) Carbamate Complexes Can Codeliver Pt(II) Drugs and Amine Containing Bioactive Molecules, *Inorg. Chem.* 59 (2020) 5182–5193. <https://doi.org/10.1021/acs.inorgchem.0c00445>.
- [37] V. Brabec, S. Karmakar, H. Kostrhunova, T. Ctvrtlikova, V. Novohradsky, D. Gibson, Platinum(IV)-Estramustine Multiaction Prodrugs Are Effective Antiproliferative Agents against Prostate Cancer Cells, *J. Med. Chem.* 63 (2020) 13861–13877. <https://doi.org/10.1021/acs.jmedchem.0c01400>.
- [38] S. Karmakar, I. Poetsch, C.R. Kowol, P. Heffeter, D. Gibson, Synthesis and Cytotoxicity of Water-Soluble Dual- And Triple-Action Satraplatin Derivatives: Replacement of Equatorial Chlorides of Satraplatin by Acetates, *Inorg. Chem.* 58 (2019) 16676–16688. <https://doi.org/10.1021/acs.inorgchem.9b02796>.
- [39] T. Yempala, T. Babu, S. Karmakar, A. Nemirovski, M. Ishan, V. Gandin, D. Gibson, Expanding the Arsenal of Pt<sup>IV</sup> Anticancer Agents: Multi-action Pt<sup>IV</sup> Anticancer Agents with Bioactive Ligands Possessing a Hydroxy Functional Group, *Angew. Chemie - Int. Ed.* 58 (2019) 18218–18223. <https://doi.org/10.1002/anie.201910014>.

- [40] P.J. Bednarski, F.S. Mackay, P.J. Sadler, Photoactivatable Platinum Complexes, *Anti-Cancer Agents Med.Chem.* 7 (2007) 75–93.  
<https://doi.org/10.2174/187152007779314053>
- [41] Y. Zhao, J.A. Woods, N.J. Farrer, K.S. Robinson, J. Pracharova, J. Kasparikova, O. Novakova, H. Li, L. Salassa, A.M. Pizarro, G.J. Clarkson, L. Song, V. Brabec, P.J. Sadler, Diazido Mixed-Amine Platinum(IV) Anticancer Complexes Activatable by Visible-Light Form Novel DNA Adducts, *Chem. Eur. J.* 19 (2013) 9578–9591.  
<https://doi.org/10.1002/chem.201300374>.
- [42] F.S. Mackay, N.J. Farrer, L. Salassa, H. Tai, R.J. Deeth, Synthesis, characterisation and photochemistry of Pt<sup>IV</sup> pyridyl azido acetato complexes, *Dalton Trans.* (2009) 2315–2325. <https://doi.org/10.1039/b820550g>.
- [43] E. Wexselblatt, D. Gibson, What do we know about the reduction of Pt(IV) pro-drugs ?, *J. Inorg. Biochem.* 117 (2012) 220–229. <https://doi.org/10.1016/j.jinorgbio.2012.06.013>.
- [44] A. Nemirovski, Y. Kasherman, Y. Tzaraf, D. Gibson, Reduction of cis,trans,cis-[PtCl<sub>2</sub>(OCOCH<sub>3</sub>)<sub>2</sub>(NH<sub>3</sub>)<sub>2</sub>] by Aqueous Extracts of Cancer Cells, *J. Med. Chem.* 50 (2007) 5554–5556. <https://doi.org/10.1021/jm070740j>
- [45] A. Lasorsa, V. Brabec, G. Natile, F. Arnesano, Activation of Platinum(IV) Prodrugs by Cytochrome c and Characterization of the Protein Binding Sites, *Mol. Pharm.* 13 (2016) 3216–3223. <https://doi.org/10.1021/acs.molpharmaceut.6b00438>.
- [46] H.P. Varbanov, S.M. Valiahd, C.R. Kowol, M.A. Jakupec, M. Galanski, B.K. Keppler, Novel tetracarboxylatoplatinum(IV) complexes as carboplatin prodrugs, *Dalton Trans.* 41 (2012) 14404–14415. <https://doi.org/10.1039/c2dt31366a>.
- [47] C.K.J. Chen, P. Kappen, D. Gibson, T.W. Hambley, trans-Platinum(IV) pro-drugs that exhibit unusual resistance to reduction by endogenous reductants and blood serum but are rapidly activated inside cells:<sup>1</sup>H NMR and XANES spectroscopy study, *Dalton Trans.* 49 (2020) 7722–7736. <https://doi.org/10.1039/d0dt01622e>.
- [48] J.A. Platts, G. Ermondi, G. Caron, M. Ravera, E. Gabano, L. Gaviglio, G. Pelosi, D. Osella, Molecular and statistical modeling of reduction peak potential and lipophilicity

- of platinum(IV) complexes, *J. Biol. Inorg. Chem.* 16 (2011) 361–372.  
<https://doi.org/10.1007/s00775-010-0731-1>.
- [49] J.J. Wilson, S.J. Lippard, Synthesis, characterization, and cytotoxicity of platinum(IV) carbamate complexes, *Inorg. Chem.* 50 (2011) 3103–3115.  
<https://doi.org/10.1021/ic2000816>.
- [50] A.R. Battle, R. Choi, D.E. Hibbs, T.W. Hambley, Platinum(IV) analogues of AMD473 (cis-[PtCl<sub>2</sub>(NH<sub>3</sub>)(2-picoline)]): Preparative, structural, and electrochemical studies, *Inorg. Chem.* 45 (2006) 6317–6322. <https://doi.org/10.1021/ic060273g>.
- [51] N.A. Kratochwil, P.J. Bednarski, Relationships between Reduction Properties and Cancer Cell Growth Inhibitory Activities of cis-Dichloro- and cis-Diiodo-Pt(IV)-ethylenediamines, *Arch. Pharm. (Weinheim)*. 332 (1999) 279–285.  
[https://doi.org/10.1002/\(SICI\)1521-4184\(19998\)332:8<279::AID-ARDP279>3.0.CO;2-1](https://doi.org/10.1002/(SICI)1521-4184(19998)332:8<279::AID-ARDP279>3.0.CO;2-1).
- [52] T.W. Hambley, A.R. Battle, G.B. Deacon, E.T. Lawrenz, G.D. Fallon, B.M. Gatehouse, L.K. Webster, S. Rainone, Modifying the properties of platinum(IV) complexes in order to increase biological effectiveness, *J. Inorg. Biochem.* 77 (1999) 3–12.
- [53] J.Z. Zhang, E. Wexselblatt, T.W. Hambley, D. Gibson, Pt(IV) analogs of oxaliplatin that do not follow the expected correlation between electrochemical reduction potential and rate of reduction by ascorbate, *Chem. Commun.* 48 (2012) 847–849.  
<https://doi.org/10.1039/c1cc16647f>.
- [54] M.R. Reithofer, A.K. Bytzek, S.M. Valiahd, C.R. Kowol, M. Groessl, C.G. Hartinger, M.A. Jakupiec, M. Galanski, B.K. Keppler, Tuning of lipophilicity and cytotoxic potency by structural variation of anticancer platinum(IV) complexes, *J. Inorg. Biochem.* 105 (2011) 46–51. <https://doi.org/10.1016/j.jinorgbio.2010.09.006>.
- [55] M.C. McCormick, K. Keijzer, A. Polavarapu, F.A. Schultz, M. Baik, Understanding Intrinsically Irreversible, Non-Nernstian, Two-Electron Redox Processes: A Combined Experimental and Computational Study of the Electrochemical Activation of Platinum(IV) Antitumor Prodrugs, *J. Am. Chem. Soc.* 136 (2014) 8992–9000.

- <https://doi.org/10.1021/ja5029765>.
- [56] K.A. Smith, J.C. Conboy, Using Micropatterned Lipid Bilayer Arrays to Measure the Effect of Membrane Composition on Merocyanine 540 Binding, *Biochim Biophys Acta*. 1808 (2011) 1611–1617. <https://doi.org/10.1016/j.bbame.2011.02.017>.
- [57] R. Köckerbauer, P.J. Bednarski, A novel approach to Preparing Water Soluble Prodrug Forms of Cisplatin Analogues Bearing Chelating Diamines, *J. Pharm. Sci.* 84 (1995) 819–823. [https://doi.org/10.1300/j456v01n03\\_06](https://doi.org/10.1300/j456v01n03_06).
- [58] M.D. Hossain, M. Haga, B. Gholamkhash, K. Nozaki, M. Tsushima, N. Ikeda, T. Ohno, Syntheses, Spectroelectrochemistry and Photoinduced Electron-Transfer Processes of Novel Ru and Os Dyad and Triad Complexes with Functionalized Diimide Ligands, *Collect. Czechoslov. Chem. Commun.* 66 (2001) 307–337. <https://doi.org/10.1135/cccc20010307>.
- [59] C. Pérez-Arnaiz, J. Leal, N. Busto, M.C. Carrión, A.R. Rubio, I. Ortiz, G. Barone, B. Díaz De Greñu, J. Santolaya, J.M. Leal, M. Vaquero, F.A. Jalón, B.R. Manzano, B. García, Role of Seroalbumin in the Cytotoxicity of cis-Dichloro Pt(II) Complexes with (N^N)-Donor Ligands Bearing Functionalized Tails, *Inorg. Chem.* 57 (2018) 6124–6134. <https://doi.org/10.1021/acs.inorgchem.8b00713>.
- [60] G.R. Fulmer, A.J.M. Miller, N.H. Sherden, H.E. Gottlieb, A. Nudelman, B.M. Stoltz, J.E. Bercaw, K.I. Goldberg, NMR chemical shifts of trace impurities: Common laboratory solvents, organics, and gases in deuterated solvents relevant to the organometallic chemist, *Organometallics*. 29 (2010) 2176–2179. <https://doi.org/10.1021/om100106e>.
- [61] SAINT v8.37, Bruker-AXS (2016), APEX3 v2016.1.0. Madison, Wisconsin, USA., n.d.
- [62] L. Krause, R. Herbst-Irmer, G.M. Sheldrick, D. Stalke, SADABS, *J. Appl. Crystallogr.* 48 (2015) 3.
- [63] L.J. Farrugia, WinGX and ORTEP for Windows: An update, *J. Appl. Crystallogr.* 45 (2012) 849–854. <https://doi.org/10.1107/S0021889812029111>.
- [64] G. M. Sheldrick, SHELX-2014, Program for Crystal Structure Refinement, University of

- Göttingen, Göttingen, Germany, 2014., (n.d.).
- [65] V.M. Ivanov, E.M. Adamova, V.N. Figurovskaya, Acid-base, spectrophotometric, and colorimetric properties of 1,2-dihydroxyantraquinone-3-sulfoacid (Alizarin Red S), *J. Anal. Chem.* 65 (2010) 473–481. <https://doi.org/10.1134/S1061934810050072>.
- [66] Gaussian 09 (Revision D.01), M. J. Frisch, G. W. Trucks, H.B Schlegel, G. E. Scuseria, M. A. Robb, J. R. Cheeseman, G. Scalmani, V. Barone, B. Mennucci, G. A. Petersson, H. Nakatsuji, M. Caricato, X. Li, H. P. Hratchian, A. F. Izmaylov, J. Bloino, G., (n.d.).
- [67] A.D. Becke, Density-functional thermochemistry. I. The effect of the exchange-only gradient correction, *J. Chem. Phys.* 96 (1992) 2155–2160.
- [68] C. Lee, W. Yang, R.G. Parr, Development of the Colle-Salvetti correlation-energy formula into a functional of the electron density, *Phys. Rev. B.* 37 (1988) 785–789.
- [69] S. Grimme, S. Ehrlich, L. Goerigk, Effect of the damping function in dispersion corrected density functional theory, *J. Comput. Chem.* 32 (2011) 1456–1465. <https://doi.org/10.1002/jcc.21759>.
- [70] P.J. Hay, W.R. Wadt, Ab initio effective core potentials for molecular calculations. Potentials for K to Au including the outermost core orbitals, *J. Chem. Phys.* 82 (1985) 299–310. <https://doi.org/10.1063/1.448975>.
- [71] A. Ehlers, A.W.; Böhme, M; Dapprich, S.; Gobbi, A.; Höllwarth, V. Jonas, K.F. Köhler, R. Stegmann, A. Veldkamp, G. Frenking, A set of f-polarization functions for pseudo-potential basis sets of the transition metals Sc-Cu, Y-Ag and La-Au, *Chem. Phys. Lett.* 208 (1993) 237–240. [https://doi.org/10.1016/0009-2614\(93\)89068-S](https://doi.org/10.1016/0009-2614(93)89068-S).
- [72] W.J. Hehre, K. Ditchfield, J.A. Pople, Self-consistent molecular orbital methods. XII. Further extensions of gaussian-type basis sets for use in molecular orbital studies of organic molecules, *J. Chem. Phys.* 56 (1972) 2257–2261. <https://doi.org/10.1063/1.1677527>.
- [73] A. V. Marenich, C.J. Cramer, D.G. Truhlar, Universal Solvation Model Based on Solute Electron Density and on a Continuum Model of the Solvent Defined by the Bulk Dielectric Constant and Atomic Surface Tensions, *J. Phys. Chem. B.* 113 (2009) 6378–

6396. <https://doi.org/10.1021/jp810292n>.
- [74] H.P. Hratchian, H.B. Schlegel, Using Hessian Updating To Increase the Efficiency of a Hessian Based Predictor-Corrector Reaction Path Following Method, *J. Chem. Theory Comput.* 1 (2005) 61–69. <https://doi.org/10.1021/ct0499783>
- [75] K.A. Connors, *Chemical kinetics. The Study of Reaction Rates in Solution*, VCH, New York, 1990.
- [76] M.E. Casida, C. Jamorski, K.C. Casida, D.R. Salahub, Molecular excitation energies to high-lying bound states from time-dependent density-functional response theory: Characterization and correction of the time-dependent local density approximation ionization threshold, *J. Chem. Phys.* 108 (1998) 4439–4449. <https://doi.org/10.1063/1.475855>.
- [77] C. Mock, I. Puscasu, M.J. Rauterkus, G. Tallen, J.E.A. Wolff, B. Krebs, Novel Pt(II) anticancer agents and their Pd(II) analogues: Syntheses, crystal structures, reactions with nucleobases and cytotoxicities, *Inorganica Chim. Acta.* 319 (2001) 109–116. [https://doi.org/10.1016/S0020-1693\(01\)00459-5](https://doi.org/10.1016/S0020-1693(01)00459-5).
- [78] F. Gumus, I. Pamuk, T. Ozden, S. Yıldız, N. Diril, E. Oksuzoglu, S. Gur, A. Ozkul, Synthesis, characterization and in vitro cytotoxic, mutagenic and antimicrobial activity of platinum(II) complexes with substituted benzimidazole ligands, *J. Inorg. Biochem.* 94 (2003) 255–262. [https://doi.org/10.1016/s0162-0134\(03\)00005-9](https://doi.org/10.1016/s0162-0134(03)00005-9)
- [79] X. He, C.M. Vogels, A. Decken, S.A. Westcott, Pyridyl benzimidazole, benzoxazole, and benzothiazole platinum complexes, *Polyhedron.* 23 (2004) 155–160. <https://doi.org/10.1016/j.poly.2003.09.020>.
- [80] J.S. Casas, A. Castiñeiras, E. García-Martínez, Y. Parajó, M.L. Pérez-Parallé, A. Sánchez-González, J. Sordo, Synthesis and Cytotoxicity of 2-(2'-Pyridyl)benzimidazole Complexes of Palladium(II) and Platinum(II), *Zeitschrift Für Anorg. Und Allg. Chemie.* 631 (2005) 2258–2264. <https://doi.org/10.1002/zaac.200570054>.
- [81] M. Serratrice, L. Maiore, A. Zucca, S. Stoccoro, I. Landini, E. Mini, L. Massai, G. Ferraro, A. Merlino, L. Messori, M.A. Cinellu, Cytotoxic properties of a new

- organometallic platinum(II) complex and its gold(I) heterobimetallic derivatives, *Dalton Trans.* 45 (2016) 579–590. <https://doi.org/10.1039/c5dt02714d>.
- [82] A.J. Canty, E.A. Stevens, Synthesis of potential platinum(II) anti-tumor complexes: Complexes containing bidentate pyridyl and imidazolyl donors, *Inorganica Chim. Acta.* 55 (1981) L57–L59. [https://doi.org/10.1016/S0020-1693\(00\)90768-0](https://doi.org/10.1016/S0020-1693(00)90768-0).
- [83] J.J. Wilson, S.J. Lippard, Synthetic Methods for the Preparation of Platinum Anticancer Complexes, *Chem. Rev.* 114 (2014) 4470–4495. <https://doi.org/10.1021/cr4004314>.
- [84] T.J. Sabo, G.N. Kaluderovic, S.R. Grguric-Sipka, F.W. Heinemann, S.R. Trifunovi, Complex compounds of platinum(IV) and O,O-dialkyl-ethylenediamine-N,N'-di-3-propanoate ligands . A structural evidence for geometry of hydrolytic product of some esters, *Inorg. Chem. Commun.* 7 (2004) 241–244. <https://doi.org/10.1016/j.inoche.2003.11.007>.
- [85] J.M. Vujic, G.N. Kaluderovic, B.B. Zmejkovski, M. Milovanovic, V. Volarevic, N. Arsenijevic, T.P. Stanojkovic, S.R. Trifunovic, Stereospecific ligands and their complexes. Part X : Synthesis, characterization and in vitro antitumoral activity of platinum(IV) complexes with O,O' -dialkyl- (S,S)-ethylenediamine-N,N'-di-2-(4-methyl)pentanoate ligands, *Inorg. Chim. Acta.* 390 (2012) 123–128. <https://doi.org/10.1016/j.ica.2012.03.048>.
- [86] D.S. U, H. Junicke, F.W. Heinemann, The crown ether influence on ligand exchange reactions of Na<sub>2</sub>PtCl<sub>6</sub> with glycine and D - (+) -alanine ; synthesis and characterization of platinum (IV) amino acid complexes, *Inorg. Chim. Acta.* 256 (1997) 87–92.
- [87] H. Schmidt, S. Schwieger, C. Wagner, G.N. Kalud, R. Paschke, A. Dietrich, T. Mueller, D. Steinborn, Platinum(IV) complexes with ethylenediamine-N,N' -diacetate diester (R<sub>2</sub>edda ) ligands: Synthesis, characterization and in vitro antitumoral activity, *Inorg. Chim. Acta.* 361 (2008) 1395–1404. <https://doi.org/10.1016/j.ica.2007.09.010>.
- [88] G.M. Rakic, S. Grguric-Sipka, G.N. Kaluderovic, M. Bette, L. Filipovi, S. Arandelovic, S. Radulovic, Z.L. Tesic, The synthesis, spectroscopic, X-ray characterization and in vitro cytotoxic testing results of activity of five new trans -platinum(IV) complexes with

- functionalized pyridines, *Eur. J. Med. Chem.* 55 (2012) 214–219.  
<https://doi.org/10.1016/j.ejmech.2012.07.019>.
- [89] W.J. Geary, The Use of Conductivity Measurements in Organic Solvents, *Coord. Chem. Rev.* 7 (1970) 81–122.
- [90] D. Gudat, A. Dogan, W. Kaim, A. Klein, Multinuclear NMR study of some organoplatinum complexes containing multifunctional azines as chelating ligands, *Magn. Reson. Chem.* 42 (2004) 781–787. <https://doi.org/10.1002/mrc.1407>.
- [91] L. Yang, D.R. Powell, R.P. Houser, Structural variation in copper (I) complexes with pyridylmethanamide ligands: structural analysis with a new four-coordinate geometry index,  $\tau_4$ , *Dalton Trans.* (2007) 955–964. <https://doi.org/10.1039/b617136b>.
- [92] G.M. Rakic, S. Grguric-Sipka, G.N. Kaluderovic, S. Gómez-Ruiz, S.K. Bjelogrić, S.S. Radulovic, Z.L. Tesic, Novel trans -dichloridoplatinum(II) complexes with 3- and 4-acetylpyridine: Synthesis, characterization, DFT calculations and cytotoxicity, *Eur. J. Med. Chem.* 44 (2009) 1921–1925. <https://doi.org/10.1016/j.ejmech.2008.11.004>.
- [93] M.J. Macazaga, J. Rodríguez, A.G. Quiroga, S. Peregina, A. Carnero, C. Navarro-ranninger, R.M. Medina, Platinum(IV) Complexes of 3- and 4-Picolinic Acids Containing Ammine or Isopropylamine Ligands – Synthesis, Characterization, X-ray Structures, and Evaluation of Their Cytotoxic Activity against Cancer Cell Lines, *Eur. J. Inorg. Chem.* (2008) 4762–4769. <https://doi.org/10.1002/ejic.200800591>.
- [94] H.O. Davies, D.A. Brown, A.I. Yanovsky, K.B. Nolan, Synthesis of trans-bis(glycinehydroxamato)platinum(II) hydrate and trans-dichlorobis(glycylglycine)platinum(II) dihydrate and the crystal and molecular structures of trans-dichlorobis(glycine)platinum(II) dihydrate and trans,trans-dichlorobis(glycinato)pl, *Inorg. Chem.* 237 (1995) 71–77.
- [95] S. Shamsuddin, C.C. Santillan, J.L. Stark, K.H. Whitmire, Z.H. Siddik, A.R. Khokhar, Synthesis, characterization, and antitumor activity of new platinum(IV) trans -carboxylate complexes: Crystal structure of [P(cis -1,4-DACH)trans-(acetate)<sub>2</sub>Cl<sub>2</sub>], *J. Inorg. Biochem.* 71 (1998) 29–35.

- [96] T.T.T. Bui, S. Dahaoui, C. Lecomte, G.R. Desiraju, E. Espinosa, The nature of halogen...halogen interactions: A model derived from experimental charge-density analysis, *Angew. Chemie - Int. Ed.* 48 (2009) 3838–3841.  
<https://doi.org/10.1002/anie.200805739>.
- [97] J. Zhang, L. Li, X. Ji, J. Sun, L. Wang, Y. Zhang, Synthesis, characterization and cytotoxicity of iodo-bridged binuclear platinum(II) complexes, *Eur. J. Med. Chem.* 45 (2010) 2634–2637. <https://doi.org/10.1016/j.ejmech.2010.01.055>.
- [98] D. Fan, X. Yang, X. Wang, S. Zhang, J. Mao, J. Ding, L. Lin, Z. Guo, A dinuclear monofunctional platinum(II) complex with an aromatic linker shows low reactivity towards glutathione but high DNA binding ability and antitumor activity, *J. Biol. Inorg. Chem.* 12 (2007) 655–665. <https://doi.org/10.1007/s00775-007-0214-1>.
- [99] M.D. Hall, K.A. Telma, K.E. Chang, T.D. Lee, J.P. Madigan, J.R. Lloyd, I.S. Goldlust, J.D. Hoeschele, M.M. Gottesman, Say no to DMSO: Dimethylsulfoxide inactivates cisplatin, carboplatin, and other platinum complexes, *Cancer Res.* 74 (2014) 3913–3922. <https://doi.org/10.1158/0008-5472.CAN-14-0247>.
- [100] M. Patra, T. Joshi, V. Pierroz, K. Ingram, M. Kaiser, S. Ferrari, B. Spingler, J. Keiser, G. Gasser, DMSO-mediated ligand dissociation: Renaissance for biological activity of N-heterocyclic-[Ru( $\eta^6$ -arene)Cl<sub>2</sub>] drug candidates, *Chem. - A Eur. J.* 19 (2013) 14768–14772. <https://doi.org/10.1002/chem.201303341>.
- [101] S. Haneda, Z. Gan, K. Eda, M. Hayashi, Ligand effects of 2-(2-pyridyl)benzazole-Pd complexes on the X-ray crystallographic structures, <sup>1</sup>H NMR spectra, and catalytic activities in Mizoroki-Heck reactions, *Organometallics.* 26 (2007) 6551–6555. <https://doi.org/10.1021/om7008843>.
- [102] J. Zhao, Z. Xu, J. Lin, S. Gou, Exploring the Hydrolytic Behavior of the Platinum(IV) Complexes with Axial Acetato Ligands, *Inorg. Chem.* 56 (2017) 9851–9859. <https://doi.org/10.1021/acs.inorgchem.7b01355>.
- [103] E. Wexselblatt, R. Raveendran, S. Salameh, A. Friedman-Ezra, E. Yavin, D. Gibson, On the stability of Pt<sup>IV</sup> pro-drugs with haloacetato ligands in the axial positions, *Chem. - A*

- Eur. J. 21 (2015) 3108–3114. <https://doi.org/10.1002/chem.201405467>.
- [104] J. Czapla-Masztafiak, A. Kubas, Y. Kayser, D.L.A. Fernandes, W.M. Kwiatek, E. Lipiec, G.B. Deacon, K. Al-Jorani, B.R. Wood, J. Szlachetko, J. Sá, Mechanism of hydrolysis of a platinum(IV) complex discovered by atomic telemetry, *J. Inorg. Biochem.* 187 (2018) 56–61. <https://doi.org/10.1016/j.jinorgbio.2018.07.012>.
- [105] V. Brabec, O. Hrabina, J. Kasparikova, Cytotoxic platinum coordination compounds. DNA binding agents, *Coord. Chem. Rev.* 351 (2017) 2–31. <https://doi.org/10.1016/j.ccr.2017.04.013>.
- [106] J. Reedijk, New clues for platinum antitumor chemistry: Kinetically controlled metal binding to DNA, *Proc. Natl. Acad. Sci. U. S. A.* 100 (2003) 3611–3616. <https://doi.org/10.1073/pnas.0737293100>.
- [107] R.N. Bose, R.D. Cornelius, R.E. Viola, Multinuclear NMR Studies and the Kinetics of Formation of Platinum(II)-Adenine Nucleotide Complexes, *J. Am. Chem. Soc.* 108 (1986) 4403–4408. <https://doi.org/10.1021/ja00275a029>.
- [108] K. Hindmarsh, D.A. House, M.M. Turnbull, The hydrolysis products of cis-diamminedichloroplatinum(II) 9. Chloride and bromide anation kinetics for some  $[\text{Pt}^{\text{II}}(\text{N})_2(\text{OH})_2]_2^+$  complexes and the structures of  $[\text{Pt}^{\text{IV}}\text{Br}_4(\text{N})_2]$  ( $(\text{N})_2 = \text{en}, \text{tn}$ ), *Inorg. Chim. Acta.* 257 (1997) 11–18.
- [109] J.L. Jestin, B. Lambert, J.C. Chottard, Kinetic study of DNA binding of cisplatin and of a bicycloalkyl- substituted (ethylenediamine)dichloroplatinum(II) complex, *J. Biol. Inorg. Chem.* 3 (1998) 515–519. <https://doi.org/10.1007/s007750050262>.
- [110] D. Wang, S.J. Lippard, Cellular processing of platinum anticancer drugs, *Nat. Rev. Drug Discov.* 4 (2005) 307–320. <https://doi.org/10.1038/nrd1691>.
- [111] M.S. Davies, S.J. Berners-Price, T.W. Hambley, Slowing of cisplatin aquation in the presence of DNA but not in the presence of phosphate: Improved understanding of sequence selectivity and the roles of mono-aquated and diaquated species in the binding of cisplatin to DNA, *Inorg. Chem.* 39 (2000) 5603–5613. <https://doi.org/10.1021/ic000847w>.

- [112] J. Raber, C. Zhu, L.A. Eriksson, Activation of anti-cancer drug cisplatin - Is the activated complex fully aquated?, *Mol. Phys.* 102 (2004) 2537–2544.  
<https://doi.org/10.1080/0026897042000275053>.
- [113] F. Legendre, V. Bas, J. Kozelka, J.-C. Chottard, A Complete Kinetic Study of GG versus AG Platination Suggests That the Doubly Aquated Derivatives of Cisplatin Are the Actual DNA Binding Species, *Chem. - A Eur. J.* 6 (2000) 2002–2010.  
[https://doi.org/10.1002/1521-3765\(20000602\)6:11<2002::AID-CHEM2002>3.0.CO;2-H](https://doi.org/10.1002/1521-3765(20000602)6:11<2002::AID-CHEM2002>3.0.CO;2-H).
- [114] J.K. Lau, B. Ensing, Hydrolysis of cisplatin — a first-principles metadynamics study, *Phys. Chem. Chem. Phys.* 12 (2010) 10348–10355. <https://doi.org/10.1039/b918301a>.
- [115] E.R. Jamieson, S.J. Lippard, Structure, recognition, and processing of cisplatin-DNA adducts, *Chem. Rev.* 99 (1999) 2467–2498. <https://doi.org/10.1021/cr980421n>.
- [116] V. Zoumpourlis, D.J. Kerr, D.A. Spandidos, Carboplatin as opposed to cisplatin does not stimulate the expression of the human immunodeficiency virus long terminal repeat sequences, *Biochem. Pharmacol.* 43 (1992) 650–654.
- [117] M. Pavelka, M.F.A. Lucas, N. Russo, On the hydrolysis mechanism of the second-generation anticancer drug carboplatin, *Chem. - A Eur. J.* 13 (2007) 10108–10116.  
<https://doi.org/10.1002/chem.200700887>.
- [118] S.J. Berners-Price, T.A. Frenkiel, U. Frey, J.D. Ranfor, P.J. Sadler, Hydrolysis Products of Cisplatin: pK, Determinations via [<sup>1</sup>H, <sup>15</sup>N] NMR Spectroscopy, *J. Chem. Soc. Chem. Commun.* (1992) 789–791.
- [119] Y. Chen, Z. Guo, S. Parsons, P.J. Sadler, Stereospecific and kinetic control over the hydrolysis of a sterically hindered platinum picoline anticancer complex, *Chem. - A Eur. J.* 4 (1998) 672–676. [https://doi.org/10.1002/\(SICI\)1521-3765\(19980416\)4:4<672::AID-CHEM672>3.0.CO;2-8](https://doi.org/10.1002/(SICI)1521-3765(19980416)4:4<672::AID-CHEM672>3.0.CO;2-8).
- [120] K. Hindmarsh, D.A. House, M.M. Turnbull, The hydrolysis products of cis-diamminedichloroplatinum(II) 9. Chloride and bromide anation kinetics for some [Pt<sup>II</sup>(N)<sub>2</sub>(OH<sub>2</sub>)<sub>2</sub>]<sup>2+</sup> complexes and the structures of [P<sup>IV</sup>Br<sub>4</sub>(N)<sub>2</sub>](N)<sub>2</sub> = en, tn), *Inorg.*

- Chim. Acta. 257 (1997) 11–18.
- [121] S.J. Barton, K.J. Barnham, A. Habtemariam, R.E. Sue, P.J. Sadler, pKa values of aqua ligands of platinum(II) anticancer complexes: [1H, 15N] and 195Pt NMR studies of cis- and trans-[PtCl<sub>2</sub>(NH<sub>3</sub>)(cyclohexylamine)], *Inorganica Chim. Acta.* 273 (1998) 8–13. [https://doi.org/10.1016/s0020-1693\(97\)05912-4](https://doi.org/10.1016/s0020-1693(97)05912-4).
- [122] J.L. Jestin, J.C. Chottard, U. Frey, G. Laurency, A.E. Merbach, Mechanism of Aquation of Bicycloalkyl-Substituted(Ethylenediamine)dichloroplatinum(II) Complexes: A Search for the Understanding of Their Differences in Antitumor Activity, *Inorg. Chem.* 33 (1994) 4277–4282. <https://doi.org/10.1021/ic00097a014>.
- [123] I. Mitra, V.P.R. B, S. Mukherjee, W. Linert, S.C. Moi, Hydrolysis theory based on density functional studies for cytotoxic Pt(II) and Pd(II) complexes with benzimidazole derivative, *Chem. Phys. Lett.* 678 (2017) 250–258. <https://doi.org/10.1016/j.cplett.2017.04.065>.
- [124] S. Mukherjee, V.P. Reddy B., I. Mitra, W. Linert, S.C. Moi, Hydrolysis mechanism of (N, N) chelated cytotoxic Pt/Pd(II)-dichloro complexes: A theoretical approach, *Chem. Phys. Lett.* 678 (2017) 241–249. <https://doi.org/10.1016/j.cplett.2017.04.069>.
- [125] M.L.. Tobe, J. Burgess, *Inorganic Reaction Mechanisms*, Longman, Essex, U.K., 1999.
- [126] J. Cooper, T. Ziegler, A Density Functional Study of SN<sub>2</sub> Substitution at Square-Planar Platinum(II) Complexes, *Inorg. Chem.* 41 (2002) 6614–6622. <https://doi.org/10.1021/ic020294k>.
- [127] J. V Burda, M. Zeizinger, J. Leszczynski, Hydration Process as an Activation of Trans- and Cisplatin Complexes in Anticancer Treatment. DFT and Ab Initio Computational Study of Thermodynamic and Kinetic Parameters, *J. Comput. Chem.* 2 (2005) 907–914. <https://doi.org/10.1002/jcc.20228>.
- [128] I. Mitra, V.P. Reddy B, S. Mukherjee, W. Linert, S.C. Moi, Hydrolysis theory based on density functional studies for cytotoxic Pt(II) and Pd(II) complexes with benzimidazole derivative, *Chem. Phys. Lett.* 678 (2017) 250–258. <https://doi.org/10.1016/j.cplett.2017.04.065>.

- [129] K.D. Cole, C.M. Tellez, R.W. Blakesley, Separation of different physical forms of plasmid DNA using a combination of low electric field strength and flow in porous media: Effect of different field gradients and porosity of the media, *Electrophoresis*. 21 (2000) 1010–1017. [https://doi.org/10.1002/\(SICI\)1522-2683\(20000301\)21:5<1010::AID-ELPS1010>3.0.CO;2-7](https://doi.org/10.1002/(SICI)1522-2683(20000301)21:5<1010::AID-ELPS1010>3.0.CO;2-7).
- [130] Z.H. Siddik, Cisplatin: Mode of cytotoxic action and molecular basis of resistance, *Oncogene*. 22 (2003) 7265–7279. <https://doi.org/10.1038/sj.onc.1206933>.
- [131] J. Halaschek-Wiener, V. Wacheck, H. Schlagbauer-Wadl, K. Wolff, Y. Kloog, B. Jansen, A novel Ras antagonist regulates both oncogenic Ras and the tumor suppressor p53 in colon cancer cells, *Mol. Med*. 6 (2000) 693–704.
- [132] X. Cao, J. Hou, Q. An, Y.G. Assaraf, X. Wang, Towards the overcoming of anticancer drug resistance mediated by p53 mutations, *Drug Resist. Updat*. 49 (2020) 100671. <https://doi.org/10.1016/j.drug.2019.100671>.
- [133] M. Kutwin, E. Sawosz, S. Jaworski, N. Kurantowicz, B. Strojny, A. Chwalibog, Structural damage of chicken red blood cells exposed to platinum nanoparticles and cisplatin, *Nanoscale Res. Lett*. 9:257 (2014) 1–6. <https://doi.org/10.1186/1556-276X-9-257>.
- [134] M. González-Bártulos, C. Aceves-Luquero, J. Qualai, O. Cussó, M.A. Martínez, S. Fernández de Mattos, J.A. Menéndez, P. Villalonga, M. Costas, X. Ribas, A. Massaguer, Pro-Oxidant Activity of Amine-Pyridine-Based Iron Complexes Efficiently Kills Cancer and Cancer Stem-Like Cells, *PLoS One*. 10 (2015) e0137800. <https://doi.org/10.1371/journal.pone.0137800>.
- [135] S. Parveen, M. Hanif, E. Leung, K.K.H. Tong, A. Yang, J. Astin, G.H. De Zoysa, T.R. Steel, D. Goodman, S. Movassaghi, T. Söhnel, V. Sarojini, S.M.F. Jamieson, C.G. Hartinger, Anticancer organorhodium and-iridium complexes with low toxicity in vivo but high potency in vitro: DNA damage, reactive oxygen species formation, and haemolytic activity, *Chem. Commun*. 55 (2019) 12016–12019. <https://doi.org/10.1039/C9CC03822A>.

[136] Y.I. Tur'yan, R. Kohen, Formal redox potentials of the dehydro-L-ascorbic acid/L-ascorbic acid system, *J. Electroanal. Chem.* 380 (1995) 273–277.

[https://doi.org/10.1016/0022-0728\(94\)03524-7](https://doi.org/10.1016/0022-0728(94)03524-7).